Applied Catalysis B: Environmental 97 (2010) 307–322

Contents lists available at ScienceDirect

Applied Catalysis B: Environmental

journal homepage: www.elsevier.com/locate/apcatb

$La_{0.8}Sr_{0.2}Ga_{0.8}Fe_{0.2}O_{3-\delta}$: Influence of the preparation procedure on reactivity toward methanol and ethanol

Alessandro Galenda[a,*], Marta Maria Natile[a,b], Luca Nodari[a], Antonella Glisenti[a]

[a] Dipartimento di Scienze Chimiche, Università di Padova, Via F. Marzolo 1, 35131 Padova, Italy
[b] ISTM-CNR, INSTM, Via F. Marzolo 1, 35131 Padova, Italy

ARTICLE INFO

Article history:
Received 17 November 2009
Received in revised form 31 March 2010
Accepted 10 April 2010
Available online 24 April 2010

Keywords:
Doped lanthanum Gallate
Perovskite
Fuel cells
Methanol
Ethanol

ABSTRACT

In this paper a strontium- and iron-doped lanthanum gallate ($La_{0.8}Sr_{0.2}Ga_{0.8}Fe_{0.2}O_3$—LSGF) is prepared by Pechini process and polyacrylamide gel method. The powders are characterized by means of X-ray Diffraction (XRD), X-ray Photoelectron Spectroscopy (XPS), Diffuse Reflectance Infrared Fourier Transform spectroscopy (DRIFT), Thermal Programmed Desorption (TPD), Thermal Programmed Reduction (TPR), BET specific surface area, UV–Vis and Mössbauer Spectroscopy (MS). The activity toward methanol and ethanol is investigated by Infrared (IR) spectroscopy and Quadrupolar Mass Spectrometry (QMS) under several conditions. XRD outcomes reveal the formation of the desired perovskite phase at 900 °C, however, small amounts of secondary phases are also present. LSGF synthesized by Pechini process is characterized by a lower amount of secondary phases. On the other hand, LSGF from polyacrylamide gel method has a higher specific surface area. XPS data show that the two samples differ for surface cations segregation, hydroxylation degree and carbonate contamination. These results are also confirmed by DRIFT and TPD measurements. MS and TPR analyses reveal the presence of a small amount of Fe(IV), which is reduced to Fe(III) with H_2 (5% in Ar) at about 450 °C and with CH_3OH vapours at 200 °C. Catalytic tests prove that methanol is mainly decomposed into H_2 and CO at 400 °C, but small amounts of CO_2 are also detected. Ethanol undergoes essentially dehydrogenation thus forming acetaldehyde and H_2. In oxidizing conditions, both alcohols are oxidized to CO_2 and H_2O at 400 °C, nevertheless, partially oxidized products are also observed. Acetaldehyde is an important product in ethanol oxidation. Under steam reforming conditions, methanol and ethanol give H_2, CO and CO_2, but acetaldehyde is also observed in ethanol steam reforming. The presence of acetaldehyde, when dealing with ethanol, suggests a difficult C–C bond break. Both the LSGF samples undergo poisoning during the reactions.

1. Introduction

In the present contribution, strontium- and iron-doped lanthanum gallates, prepared by means of different procedures, are investigated with respect to methanol and ethanol under oxidizing and steam reforming conditions.

Stoichiometrically, the steam reforming reactions of methanol and ethanol (SRM and SRE, respectively) can be represented by:

$$CH_3OH + H_2O \rightleftarrows 3H_2 + CO_2 \quad (1)$$

$$CH_3CH_2OH + 3H_2O \rightleftarrows 6H_2 + 2CO_2 \quad (2)$$

While the oxidation reactions depend on the oxygen content:

$$CH_3OH + 3/2O_2 \rightleftarrows 2H_2O + CO_2 \quad (3)$$

$$CH_3OH + O_2 \rightleftarrows CO + 2H_2O \quad (4)$$

$$CH_3OH + 1/2O_2 \rightleftarrows CO_2 + 2H_2 \quad (5)$$

$$CH_3CH_2OH + 3/2O_2 \rightleftarrows 3H_2 + 2CO_2 \quad (6)$$

$$CH_3CH_2OH + 3/2O_2 \rightleftarrows 2H_2 + H_2O + CO + CO_2 \quad (7)$$

$$CH_3CH_2OH + O_2 \rightleftarrows CH_4 + CO_2 + H_2O \quad (8)$$

$$CH_3CH_2OH + 1/2O_2 \rightleftarrows CH_3CHO + H_2O \quad (9)$$

Despite the apparent simplicity, these processes are complex and proceed via different intermediates which could produce undesirable by-products; several reaction pathways are in fact possible depending on the catalyst and on the reaction conditions:

1) Decomposition or cracking, eventually followed by the steam reforming

$$CH_3OH \rightleftarrows 2H_2 + CO \quad (10)$$

* Corresponding author. Tel.: +39 049 8275174; fax: +39 049 8275161.
E-mail address: alessandro.galenda@unipd.it (A. Galenda).

0926-3373/$ – see front matter © 2010 Elsevier B.V. All rights reserved.
doi:10.1016/j.apcatb.2010.04.004

this can also proceed via methyl formate as an intermediate:

$$2CH_3OH \rightleftarrows HCOOCH_3 + 2H_2 \quad (10a)$$

$$HCOOCH_3 \rightleftarrows 2CO + 2H_2 \quad (10b)$$

$$CO + H_2O \rightleftarrows CO_2 + H_2 \quad (11)$$

$$CH_3CH_2OH \rightleftarrows CH_4 + CO + H_2 \quad (12)$$

$$CH_4 + 2H_2O \rightleftarrows CO_2 + 4H_2 \quad (13)$$

2) Dehydrogenation to the aldehyde eventually followed by decarbonylation or steam reforming

$$CH_3OH \rightleftarrows H_2 + H_2CO \quad (14)$$

$$H_2CO + H_2O \rightleftarrows 2H_2 + CO_2 \quad (15)$$

$$CH_3CH_2OH \rightleftarrows H_2 + CH_3CHO \quad (16)$$

$$CH_3CHO \rightleftarrows CH_4 + CO \quad (17)$$

$$CH_3CHO + H_2O \rightleftarrows 3H_2 + 2CO \quad (18)$$

3) Decomposition to ketones eventually followed by steam reforming

$$2CH_3CH_2OH \rightleftarrows CH_3COCH_3 + 3H_2 + CO \quad (19)$$

$$CH_3COCH_3 + 2H_2O \rightleftarrows 5H_2 + 3CO \quad (20)$$

4) Steam reforming to syngas

$$CH_3CH_2OH + H_2O \rightleftarrows 4H_2 + 2CO \quad (21)$$

5) Methanation

$$CO + 3H_2 \rightleftarrows CH_4 + H_2O \quad (22)$$

$$CO_2 + 4H_2 \rightleftarrows CH_4 + 2H_2O \quad (23)$$

Among these reactions those causing surface coking have to be avoided:

$$CH_4 \rightleftarrows 2H_2 + C \quad (24)$$

$$2CO \rightleftarrows C + CO_2 \quad (25)$$

As well as the dehydration to ethylene which is followed by polymerization to form coke:

$$CH_3CH_2OH \rightleftarrows C_2H_4 + H_2O \quad (26)$$

$$C_2H_4 \rightarrow \text{coke} \quad (27)$$

In view of the high technological importance of these reactions, alcohol oxidation and steam reforming are rather investigated in oxides and metal/oxide systems [1–4]. In spite of this, the reactivity of perovskite-based oxides with respect to alcohols still needs to be further studied [5–8]. The perovskite-activated oxidation and steam reforming of methanol and ethanol should be considered as a significant opportunity in view of the application of these materials as catalysts or sensors.

Due to their peculiar properties (electronic and/or ionic conductivity, thermal and chemical stability, low environmental impact and cost, etc.) and to the possibility of tuning the chemical and physical behaviour by choosing composition, doping, preparation procedures, activation treatments etc., perovskites are being carefully considered in several applications and devices. Among these, Solid Oxide Fuel Cells (SOFCs) are particularly interesting. In particular, thanks to the rather high ionic conductivity even at 500–700 °C, perovskites may be very promising in Intermediate Temperature Solid Oxide Fuel Cells (IT-SOFCs).

As a general consideration, a fuel cell is an electrochemical device capable of converting chemical into electrical energy. In its simplest view, it is made of an anode (where the oxidation of fuel occurs), a cathode (reduction of oxidant) and an electrolyte which connects the two electrodes.

If an ideal process occurs, the obtained energy only depends on the ideal potential of the cell (i.e. by the fuel-oxidant couple). However, in a real device, several types of irreversible losses cause a decrease in cell efficiency. These losses are due to polarization phenomena, overpotential and ohmic losses and depend on the electrodes (electrochemical reactions and electrode conductivities) and to the electrolytes (ionic conductivity). Moreover, the working temperature affects the described phenomena.

High temperature SOFCs usually work at about 800–1100 °C in order to guarantee an adequate ionic conductivity to the Yttria Stabilized Zirconia (YSZ) electrolyte. Less relevant problems related to the long-term stability on repeated start/stop cycles, or to the choice of materials for seals or interconnect, should be warranted by operating at lower temperature. At this purpose, new materials are being investigated for the IT-SOFCs.

Several parameters and properties have to be considered for an accurate choice of the materials for a SOFC. Beside the chemical properties of the selected materials, their compatibility in the assembled device is fundamental. Electrodes and electrolyte, as an example, should have a similar thermal expansion coefficient to avoid thermal breaks. Furthermore, chemical reactions at interface (frequent at high operating temperatures), can produce undesired phases which generally reduce the electrical conductivity (i.e. the cell efficiency).

The more suitable electrolyte materials for IT-SOFC are [9]: doped ceria and perovskite-based oxides. Ceria or doped-ceria based materials also show high ionic conductivity; nevertheless, the partial reduction of cerium (IV) to cerium (III) introduces a harmful electronic conductivity. Perovskite-based oxides seem to match most of the required properties for a good electrolyte. They are, in fact, observed to be stable both under reducing and oxidizing atmosphere. Among the investigated ones, Strontium and Magnesium doped Lanthanum Gallates (LSGM) systems seem to be very promising as ionic conductors at intermediate temperature [10,11]. In particular, $La_{0.8}Sr_{0.2}Ga_{0.8}Mg_{0.2}O_{3-\delta}$ should allow the best performance.

Taking into consideration this point, the electrode materials should be set in order to guarantee, beside the electrochemical properties, the best compatibility with LSGM [12,13].

In this paper, as above mentioned, a strontium and iron doped lanthanum gallate ($La_{0.8}Sr_{0.2}Ga_{0.8}Fe_{0.2}O_3$—LSGF) is synthesized and its reactivity with respect to methanol and ethanol, alcohol oxidation and steam reforming is investigated. The chemical and structural similarity with $La_{0.8}Sr_{0.2}Ga_{0.8}Mg_{0.2}O_{3-\delta}$ guided the choice of the specimen type and composition, $La_{0.8}Sr_{0.2}Ga_{0.8}Fe_{0.2}O_3$. In this way, cations interdiffusion and thus interfacial interactions and the formation of unwanted minor phases should be minimized.

Beside the device materials, the fuel-oxidant couple also plays a significant role in the FCs operations. Usually, oxygen from air is the more reasonable solution for the oxidant, while the choice of the fuel opens to several opportunities. Hydrogen is the main candidate, but the technology for its production, storage and transportation is nowadays not favourable. Because of this reason, many studies are carried out to investigate alternative fuels. One of the advantages of the SOFCs is the possibility of using different fuels. At this purpose, light alcohols, such as methanol and ethanol are considered a good chance because the storage and transportation technologies are well consolidated; moreover, alcohol production from biomasses should also be considered.

Strontium- and iron-doped lanthanum gallate was already investigated in the literature, thanks to its mixed electronic-ionic conductivity, as semipermeable membrane in methane partial oxidation process [14,15]. Until now, in contrast, the activity in

reactions (such as alcohols oxidation and steam reforming) relevant in SOFC technology need to be further considered. The investigation of perovskite reactivity under different conditions is very important. The design of a fuel cell system involves more than the optimizing of the fuel cell section with respect to efficiency or economics. It involves minimizing the cost of electricity (or heat and electric products as in a cogeneration system) within the constraints of the desired application. For most applications, this requires that the fundamental processes be integrated into an efficient plant with low capital cost. Often these objectives are conflicting, so compromises are required and fuel flexibility can offer an opportunity.

Also the synthetic route plays a key role in the properties of the materials, deeply affecting the chemical and physical properties; in particular, the surface properties are of primary importance in heterogeneous catalysis.

The synthesis of a mixed oxide is classically carried out by means of the so-called "ceramic route" [16]. It involves intimate mechanical mixing of oxides, carbonates, acetates or nitrates and repeated grinding and heating cycles to achieve the complete reaction between all reactants. However, despite the advantage of its simplicity, this technique has clear disadvantages since it produces large grains (1–10 μm, usually characterized by very low specific surface areas) and requires multiple thermal treatments (typically at 1300–1700 °C) and grindings. As a consequence, uncontrolled crystallites growth can occur, which could induce chemical and grain-size non-uniformity. Synthesis using wet chemistry can overcome many of these disadvantages. The homogeneity of the product is expected to increase because of the cations mixing occurs at the molecular level; the formation of the desired phase should thus be realized at lower temperature. Moreover, wet chemical procedures are usually very reproducible.

Among the different preparation procedures, the Pechini and the polyacrylamide gel methods were selected to investigate the influence of the preparation procedure on the properties and reactivity of LSGF. These methods, in fact, involve the formation of stable metal–ligand complexes and their dispersion into a homogeneous means such as a polymer. The thermal treatments allow to decompose the polymer network and to obtain the ceramic powder [16–21].

The obtained compounds were characterized by means of X-ray Diffraction (XRD), X-ray Photoelectron Spectroscopy (XPS), Diffuse Reflectance Infrared Fourier Transform spectroscopy (DRIFT), Thermal Programmed Desorption (TPD), Thermal Programmed Reduction (TPR), BET specific surface area, UV–Vis and Mössbauer Spectroscopy (MS).

The reactivity with respect to methanol and ethanol was investigated under different conditions (pure alcohol vapours, in presence of oxygen and under steam reforming conditions) by means of Quadrupolar Mass Spectrometry (QMS) and Infrared Spectroscopy.

2. Experimental

$La_{0.8}Sr_{0.2}Ga_{0.8}Fe_{0.2}O_{3-\delta}$ was prepared by Pechini process (LSGF Pec, hereafter) and by polyacrylamide gel method (LSGF Gel, hereafter), starting from La_2O_3 (Aldrich, 99.9%), $SrCO_3$ (Aldrich, 99.9+%), Fe (powder, Aldrich, -325 mesh, 99.9+%) and $Ga(acac)_3$ (Strem 99.99+% Ga).

2.1. Synthesis by Pechini process

In the Pechini process [22], citric acid (anhydrous reagent ACS, Acros Organics, 99.5%) and ethylene glycol (Acros Organics, 99+%), each one with molar ratio 1.5:1 with respect to the total amount of cations, were added to a clear aqueous solution obtained by the mineralization (with HNO_3) of the appropriate amounts of the cation precursors. The obtained solution was then heated at 70–80 °C to evaporate the aqueous solvent and obtain the gel. The mixture was then slowly heated at 110 °C for 1 h (to complete the solvent evaporation) and at 400 °C for 2 h to remove most of the polymeric network [21]. The obtained powder was further calcined at 900 °C for 5 h in order to achieve the desired crystallographic phase. After this, a dark brown-black powder was obtained.

2.2. Synthesis by polyacrylamide gel method

In the polyacrylamide gel method, the metal cations solution (obtained by mineralization of the appropriate amounts of the cation precursors with HNO_3) was basified with an ammonia solution until pH 7, then, a stoichiometric amount of EDTA (with respect to the total amount of cations) was added to the solution. After this, Acrylamide (6 g) (98.5% Acros Organics) and N,N′ methylenebisacrylamide (1 g, as cross-linker) (96% Acros Organics) were added to the solution. The mixture was heated at 80 °C and H_2O_2 was added as polymerization starter. The amounts of acrylamide and N,N′ methylenebisacrylamide are not directly related to the amount of cations, since polyacrylamide should only act as a dispersing agent. The acrylamide/N,N′ methylenebisacrylamide ratio affects the pore dimensions in polyacrylamide gel; nevertheless, it seems not to influence the final grain dimensions [16–18]. After the polymerization reaction, the gel was dehydrated at 110 °C and slowly heated up at 400 °C for 2 h.

The obtained powder was further calcinated at 900 °C for 5 h in order to achieve the desired crystallographic phase. After this, a dark brown-black powders was obtained.

3. Measurements

The XPS investigations were carried out with a Perkin Elmer Φ 5600ci Multi Technique System equipped with a double anode (Mg–Al) and a monochromatic Al anode working at 300 W as X-ray source.

The spectrometer was calibrated by assuming the binding energy (BE) of the Au $4f_{7/2}$ line to be 84.0 eV with respect to the Fermi level. Both extended spectra (survey: 187.85 eV pass energy, 0.5 eV step^{-1}, 0.05 s step^{-1}) and detailed spectra (for La3d, Sr3d, Ga2p, Fe2p, O1s and C1s: 11.75 eV pass energy, 0.1 eV step^{-1}, 0.1 s step^{-1}) were collected by means of a monochromatic Al Kα source. The standard deviation in the BE values of the XPS line is 0.10 eV. The atomic percentage, after a Shirley-type background subtraction [23] was evaluated by using the PHI sensitivity factors [24]. The peak positions were corrected for the charging effects by considering the C 1s peak at 285.0 eV and evaluating the BE differences.

The XRD analyses were performed by means of a Bruker D8 Advance diffractometer with Bragg-Brentano geometry using a Cu Kα radiation (40 kV, 40 mA, λ = 0.154 nm). The phase compositions and the crystallite sizes of the powders were determined with great accuracy by Rietveld's powder structure refinement analysis of XRD data, by using the MAUD (Material Analysis Using Diffraction) software [25]. The required crystallographic data were taken from ICSD (Inorganic Crystal Structure Database, v. 2007, Fachinformationszentrum, Karlsruhe, Germany).

The IR spectra were collected in a Bruker Tensor 27 spectrophotometer accumulating 32 scans at a resolution of 4 cm^{-1} for the measurements in diffuse reflectance mode (characterization of the samples), and of 1 cm^{-1} for the measurements in transmittance mode (activity tests).

The spectra acquired in reflectance mode are displayed in Kubelka-Munk units [26,27] using KBr as a reference. Anhydrous

Table 1
Weight Hourly Space Velocity (WHSV, weight of alcohol per gram of catalyst per hour) values employed in the catalytic tests.

Test conditions	WHSV (h^{-1})
Pure methanol	18
Methanol–O_2	24
Methanol 1 M	1
Pure ethanol	22
Ethanol–O_2	27
Ethanol 1 M	1

KBr was used as reference in all the characterization measurements (the KBr spectrum was preliminary collected as a background). For each DRIFT measurement, about 50 mg of the sample were loaded in the sample cup of a low-temperature reaction chamber (CHC) installed in the Praying Mantis accessory for diffuse reflectance infrared spectroscopy (Harrick Scientific Corporation) and fitted with ZnSe windows. The temperature of the powder was checked by means of a thermocouple inserted into the sample holder directly in contact with the powder. Before measurements, the powder was kept in argon flow to eliminate water traces until a stable IR spectrum was obtained (ca. 30 min).

The spectra acquired in transmittance mode were performed employing a flow chamber for gas analysis, fitted with NaCl windows. The spectrum of the chamber in argon flow was used as background.

Mass data were obtained by means of a System Genesys I 200D by European Spectrometry Systems. The obtained mass spectra were corrected for the multi-contributions taking into account the fragmentation patterns for each investigated compound. The mass spectra library was realized analyzing one by one the reactants and the obtained products.

The catalytic tests were carried out by loading about 40 mg of the sample in a "U" shaped glass reactor; the temperature was checked by means of a thermocouple inserted into the reactor. In each test, the reactor was fed with vapours of methanol, ethanol or vapours from aqueous solutions (1 M) of the alcohols, carried by a pure argon flow or by a mixture argon–oxygen (in the oxidation tests); the gas flows were controlled by MKS mass flow controllers. The effluent gases from the reactor reached the FTIR and the QMS for the analysis.

The feed reservoir was constantly kept at 19 °C. Taking into account this physical parameter, a series of thermodynamic calculations were made to obtain the amount of evaporated alcohols per minute. In detail, the thermodynamic calculations were made using AspenPlus software taking into account a "gamma-fi"-type model and employing the Redlich–Kwong equation for the determination of the fugacity coefficients, and the NRTL (Non-Random Two Liquid) for the activity coefficients. The obtained values were also experimentally verified by means of repeated control tests. Based on this, the Weight Hourly Space Velocity (WHSV, weight of alcohol per gram of catalyst per hour) for the three investigated conditions are calculated and resumed in Table 1.

The tests were performed for 25 min at several temperatures between RT and 400 °C; during this time, the system always reaches a steady state.

The experimental set-up was tested in the absence of catalyst under the different conditions (with respect to pure alcohol vapours, in oxidizing and steam reforming conditions) in order to verify that no spurious conversion of alcohols occurs. The experimental results confirm the absence of alcohol conversion due to the test conditions.

Temperature Programmed Reduction (TPR), Temperature Programmed Desorption (TPD) and BET specific surface area measurements were performed with an Autochem II 2010 Micromeritics,

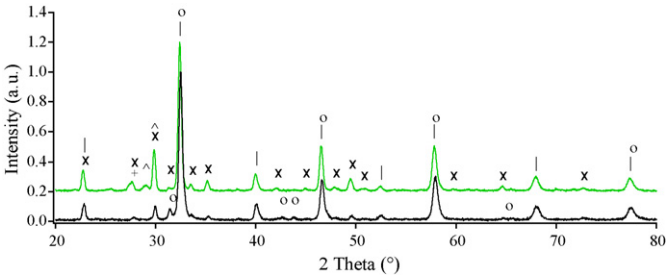

Fig. 1. XRD patterns for LSGF Pec (black) and LSGF Gel (green). The markers stand for: $La_{0.8}Sr_{0.2}Ga_{0.8}Fe_{0.2}O_3$ (|), $SrLaGaO_4$ (o), $SrLaGa_3O_7$ (×), $La(OH)_3$ (+) and La_2O_3 (^). The spectra are shifted for a better comprehension. (For interpretation of the references to color in this figure legend, the reader is referred to the web version of the article.)

equipped with a TCD detector. The TPR measurements were carried out in a quartz reactor by using 50 mg of sample and heating from RT to 900 °C at 10 °C min^{-1} under a constant flow of H_2 5% in Ar (50 ml min^{-1}). TPD measurements were performed on 0.1 g of sample by heating from RT to 900 °C at 10 °C/min under pure He stream (50 ml min^{-1}). TPD and TPR samples were previously outgases with He flow (50 ml min^{-1}) for 2 h at RT. The TPD measurements were also monitored with mass spectrometry by connecting System Genesys I 200D to the Autochem II 2010 outlet. The specific surface areas were determined (BET single point method) by means of N_2 absorption at liquid nitrogen temperature on samples previously outgassed at 350 °C for 2 h under helium flow.

Mössbauer spectroscopy analyses (MS) were performed on a conventional constant-acceleration spectrometer, with a room temperature Rh matrix ^{57}Co source (nominal strength 1850 MBq).

The hyperfine parameters isomer shift (δ), quadrupole splitting (Δ), full line-width at half-maximum (Γ), expressed in mm/s, were obtained by means of standard least-squares minimization techniques. The spectra were fitted with Lorentzian line shapes with the minimum number of doublets. It was assumed that, in all the spectra, each hyperfine parameter was affected by the same error, postulated as the maximum error over all measurements. A deviance of ±0.03 mm/s from the obtained value was assigned to δ, Δ and Γ and ±5% to Areas (A). Isomer shift is quoted relative to metallic iron at room temperature. Low-temperature spectra were collected by an ARS® closed circuit cryostat. The spectra were collected at 298 K (RT) and at 11 K.

The UV–Vis measurements were performed with a Varian CARY 5E UV–Vis–NIR spectrophotometer operating in reflectance mode. The spectra were collected from 200 to 800 nm.

4. Results and discussion

4.1. Characterization

The XRD analysis indicates that $La_{0.8}Sr_{0.2}Ga_{0.8}Fe_{0.2}O_3$ is the main phase in both the samples but reflections of other phases ($SrLaGaO_4$, $SrLaGa_3O_7$, La_2O_3 and $La(OH)_3$) are also present in different amounts (Fig. 1). From the XRD Rietveld refinement, the weight fractions of the different phases were obtained (Table 2).

The presence of $SrLaGaO_4$ and $SrLaGa_3O_7$ as secondary phases is not surprising dealing with Sr-doped lanthanum gallate and was observed by many Authors who made use of different synthetic procedures [28–30]. Kharton et al. [31] stated that for low Sr contents, the amount of $SrLaGa_3O_7$ depends on processing conditions, while, at low Fe concentrations, it may be partially affected by kinetic factors. As a general consideration, the presence of secondary phases

Table 2
XRD compositions obtained for LSGF Gel and Pec.

Sample	Main phase	%wt	Lattice	Minor phases	%wt	Lattice
LSGF Gel	$La_{0.8}Sr_{0.2}Ga_{0.8}Fe_{0.2}O_3$	67	Orthorhombic			
				$SrLaGa_3O_7$	30	Tetragonal
				La_2O_3	<2	Hexagonal
				$La(OH)_3$	<1	Hexagonal
LSGF Pec	$La_{0.8}Sr_{0.2}Ga_{0.8}Fe_{0.2}O_3$	79	Orthorhombic			
				$SrLaGa_3O_7$	11	Tetragonal
				$SrLaGaO_4$	10	Tetragonal

is influenced by the preparation conditions whenever the dopant amounts are low, and by dopants if they are present in higher concentrations. Pechini process seems to guarantee higher crystallographic purity: in LSGF Pec, both $SrLaGa_3O_7$ and $SrLaGaO_4$ are present in equal amount, while in LSGF Gel, $SrLaGaO_4$ is not detected but $SrLaGa_3O_7$ is almost threefold that observed in LSGF Pec. It is important to note that the synthetic procedure also significantly influences the crystallite sizes. The perovskite prepared by Pechini process is characterized by smaller crystallites (64 nm) than the one prepared by Gel method (94 nm). The BET measurements evidence a wider specific surface area for LSGF Gel (6.9 m^2/g) than for LSGF Pec (4.4 m^2/g).

La 3d XP peak positions (Table 3) and shape (Fig. 2) agree with the literature data reported for perovskite-type materials [32–38]; the shake-up contributions confirm the presence of La(III). Concerning the Sr3d photoelectronic peak (Fig. 2 and Table 3), the fitting procedure suggests the presence of more overlapping doublets and thus of different strontium compounds. In detail, the first contribution ($Sr3d_{5/2}$ at about 132.0 eV, ~36% of the total Sr XPS amount), is compatible with Sr^{2+} in the perovskite phase. A second contribution at about 133.3 eV (~48%) is due to $SrCO_3$ [39,40], (the attitude of Sr toward surface segregation and carbonate formation by interaction with atmospheric CO_2, is well known). The last one, at about 134.0 eV (~16%) is attributed to strontium oxide [41].

$Ga2p_{3/2}$ and Fe2p peak positions and shapes are consistent with how expected for Ga(III) and Fe(III) compounds, respectively (Fig. 2 and Table 3) [24,32–34,38].

Concerning the O1s XP peak (Fig. 2 and Table 3), the fitting procedure in LSGF Pec shows three contributions. The first one, at about 529.2 eV, agrees with oxygen in the perovskite lattice [32–34], the second one, at 531.0 eV, is ascribed to oxygen in the pure oxides and hydroxides, while the last one, at 532.0 eV, is due to the hydroxyl groups and carbonate species [38–41]. Carbonates are also confirmed by the contribution at 289.9 eV in C1s peak (Fig. 2) [32–34]. The O1s signal from LSGF Gel can be also convoluted into the same contributions but the component at 531.0 eV is present in higher amount.

Table 3 also summarizes the XPS and nominal compositions (calculated from the metal precursors weighted amounts) for LSGF Pec and Gel. The XPS and nominal compositions are shown on oxide basis (first row for each sample) and on only metal basis (second row). Both the compounds are always richer in oxygen than the nominal composition; this is not surprising and can be explained taking into account the hydroxyls surface terminations and the presence of carbonate groups. Concerning the metal cations, for both samples, strontium is clearly overabundant when compared to the nominal amount. This behaviour was already observed in similar compounds [33] and is caused by the basic properties of Sr and its tendency to segregate in surface and react with atmospheric CO_2.

Lanthanum and iron amounts agree with the nominal values and only slight differences can be revealed in LSGF Gel for lanthanum (slight decrease) and in LSGF Pec for iron (slight increase). Finally, gallium tends to diffuse in to the bulk; this behaviour is more evident for LSGF Pec.

LSGF Pec and Gel were analyzed by diffuse reflectance infrared spectroscopy at several temperatures between RT and 300 °C. Fig. 3 displays the spectra obtained for LSGF Gel and Pec. Both samples show an intense absorption band (not shown) from 650 to 850 cm^{-1} caused by the lattice vibration modes [42]. A slight difference can be observed between the spectra of the two samples in the spectral region of the carbonate species (Fig. 3a). Two main signals are observed at 1400 and 1480 cm^{-1} in the LSGF Gel whereas in the LSGF Pec the main contribution is around 1440 cm^{-1} with a broad tail at higher wavenumbers and a shoulder at 1400 cm^{-1}. These peaks are attributed to monodentate and bulk-like carbonates [43–54]; the different shape suggests a different distribution of carbonate species. The observed species can derive from the interaction of carbon dioxide with the basic sites present on the powder surface.

Fig. 3b shows the spectra obtained in the region 1250–1700 cm^{-1} for LSGF Gel at different temperatures. In the spectrum at 200 °C the growth of a new band at 1580 cm^{-1} and the increase of the shoulder at about 1360 cm^{-1} are evident. The observed signals are related to the partial transformation from monodentate carbonate into bidentate. This behaviour agrees with the formation of new acidic sites as a consequence of the water and hydroxyl groups desorption. The contributions of bidentate carbonates decrease at 300 °C thus indicating their thermal decomposition. The spectra obtained for LSGF Pec (not shown for sake of brevity) appear very similar.

Finally, a weak broad band can be observed between 3000 and 3600 cm^{-1} in both samples (Fig. 3c). The band shape and position is consistent with the presence of different species such as H-bound hydroxyl groups, and molecularly chemisorbed water [55–57]. In LSGF Gel sample a peak at 3610 cm^{-1} can be related with isolated hydroxyl on lanthanum and gallium cations [58–60].

Measurements performed at higher temperatures on LSGF Gel and Pec (until 300 °C, here not shown for sake of brevity) show the attenuation of the O–H stretching band, caused by the desorption of molecularly adsorbed water and condensation of hydroxyls. On the other hand, the O–H stretching at 3610 cm^{-1} remains essentially the same in LSGF Gel confirming its attribution to isolated hydroxyl groups.

The results of TPD–QMS measurements carried out on LSGF Gel and Pec are shown in Fig. 4. Both samples release water and carbon dioxide (no other species were detected in relevant amounts) as a function of temperature. Significant differences are evident between the two desorption profiles. Concerning LSGF Gel, the outcomes suggest a continuous desorption of molecularly absorbed water and condensation of hydroxyl groups from the sample surface from about 50 to 250 °C. Water is also desorbed at 350 °C with a well defined peak. This could be due to the condensation of more strongly bound hydroxyl groups, and could be related to the OH groups responsible for the IR peak at 3610 cm^{-1}. In the low temperature range (from 50 to about 370 °C), the sample also desorbs a small amount of CO_2. As already mentioned, the thermal stability of carbonate species changes according with the strength of the bond with the substrate. Therefore, the observed desorption can be due to the removal of mono- and biden-

Table 3
XPS peak positions (binding energy, BE, eV) and compositions (atomic%, oxide-based and only metal-based compositions) obtained for LSGF Gel and Pec. The binding energies obtained from fitting procedure are reported for oxygen and strontium.

Sample	BE (eV)								
	$La3d_{5/2}$	$Sr3d_{5/2}$			$Ga2p_{3/2}$	$Fe2p_{3/2}$	O1s		
LSGF Pec	834.8	132.0	133.3	134.0	1117.6	710.9	529.2	531.0	532.0
LSGF Gel	834.7	132.0	133.3	134.0	1117.8	711.1	529.3	531.0	532.2
		XP and nominal composition (atomic%)							
		La		Sr		Ga		Fe	O
LSGF Pec		12		5		7		4	72
		41		19		25		15	
LSGF Gel		10		7		9		2	72
		35		24		33		8	
Nominal		16		4		16		4	60
		40		10		40		10	

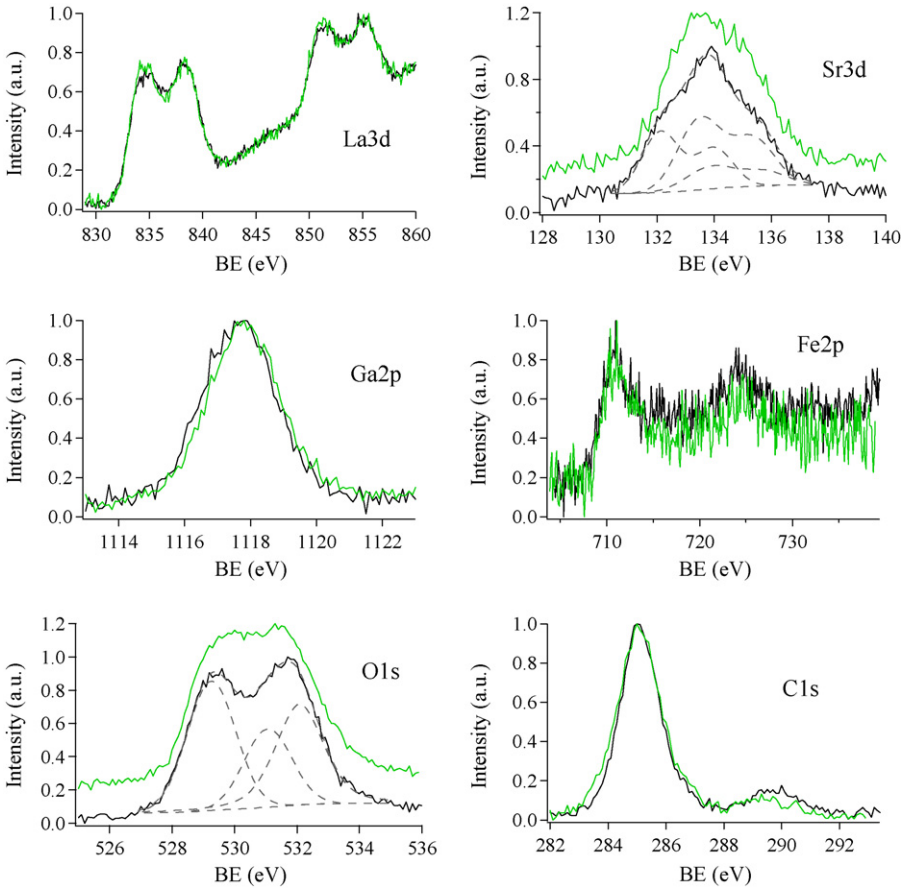

Fig. 2. XP spectra obtained for La3d, Sr3d, Ga2p, Fe2p, O1s and C1s for LSGF Pec (black) and Gel (green). The deconvoluted curves are also shown for Sr3d and O1s in LSGF Pec. All spectra are normalized with respect to their maximum value. (For interpretation of the references to color in this figure legend, the reader is referred to the web version of the article.)

Table 4
Mössbauer parameters for room-temperature (RT) and low-temperature (11 K) measurements on LSGF Pec. δ: isomeric shift; Δ: quadrupole splitting; Γ: full-width at half-height; A: relative area; δ is quoted to metallic α-iron.

Sample	T (K)	δ (mm/s)	Δ (mm/s)	Γ (mm/s)	A (%)	Attribution
LSGF Pec as prepared	RT	0.36 ± 0.03	0.18 ± 0.03	0.41 ± 0.03	79 ± 5	Fe(III) site 1
		−0.07 ± 0.03	0.17 ± 0.03	0.40 ± 0.03	21 ± 5	Fe(IV)
	11	0.42 ± 0.03	0.19 ± 0.03	0.56 ± 0.03	85 ± 5	Fe(III) site 1
		−0.13 ± 0.03	0.14 ± 0.03	0.32 ± 0.03	15 ± 5	Fe(V)
LSGF Pec after reduction	RT	0.36 ± 0.03	0.22 ± 0.03	0.39 ± 0.03	90 ± 5	Fe(III) site 1
		0.32 ± 0.03	1.06 ± 0.03	0.31 ± 0.03	10 ± 5	Fe(III) site 2
	11	0.42 ± 0.03	0.20 ± 0.03	0.48 ± 0.03	82 ± 5	Fe(III) site 1
		0.33 ± 0.03	0.90 ± 0.03	0.48 ± 0.03	18 ± 5	Fe(III) site 2

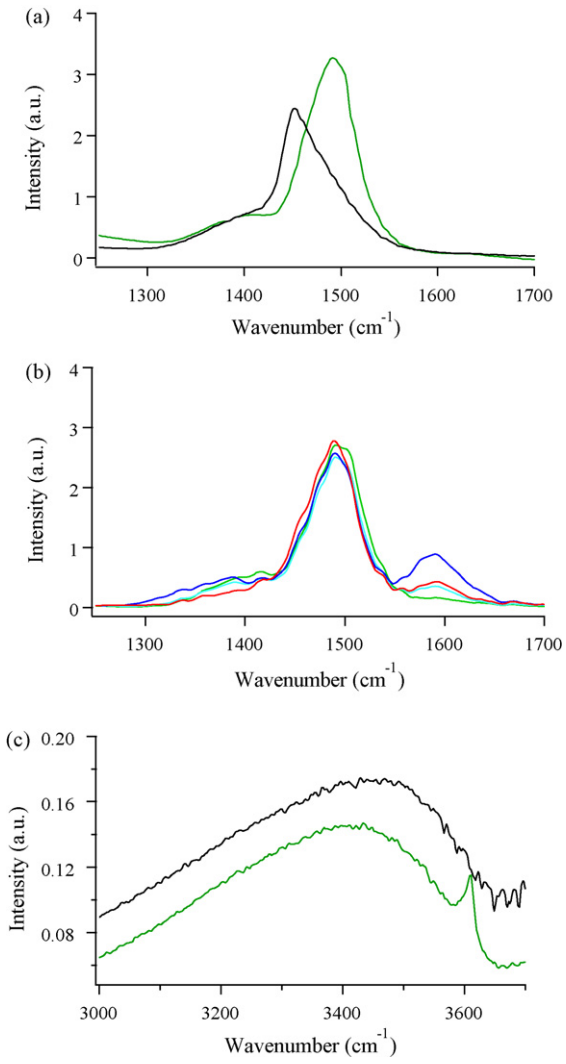

Fig. 3. DRIFT spectra obtained at RT for LSGF Gel (green) and Pec (black). Regions between 1250 and 1700 cm^{-1} (a), and between 3000 and 3700 cm^{-1} (c). (b) DRIFT spectra obtained for LSGF Gel at several temperatures in the region between 1250 and 1700 cm^{-1}. (green) RT, (light blue) 100 °C, (blue) 200 °C, (red) 300 °C. (For interpretation of the references to color in this figure legend, the reader is referred to the web version of the article.)

tate carbonates [61–63]. Carbon dioxide is also released at higher temperature. From about 530 until 830 °C, a broad and intense signal can be related to the decomposition of bulk-like carbonates [54,63].

Concerning LSGF Pec, water arising from molecularly adsorbed water and condensation of hydroxyl groups is desorbed from 50 to 300 °C. A small amount of water is also desorbed at 415 °C, as a consequence of the condensation of more strongly bound hydroxyls. The QMS data indicate the desorption of CO_2 from 50 to 300 °C. The main CO_2 desorption occurs from 530 to 830 °C. The last desorption peak, in particular, shows a different shape with respect to that in LSGF Gel: two maxima are evident at about 715 and 780 °C whereas a broad band was observed in the LSGF Gel sample. Concerning CO_2, in particular, the paths mainly differ in the range 650–750 °C, where a more relevant desorption is evident in LSGF Pec. The contributions observed in the range 530–830 °C are due to bulk-like carbonates, and the observed differences suggest a different distribution of these species. DRIFT characterization also indicates different types of carbonates (monodentate, bidentate and bulk-like) in the region between 1300 and 1700 cm^{-1} (Fig. 3a and b). In particular, a more evident contribution at about 1480 cm^{-1} is observed in LSGF Gel. A thermal evolution of carbonate species into more tightly bound carbonates (peaks at higher temperatures) can also play a role.

Since the synthetic procedures involve a final thermal treatment at 900 °C (equal to the highest temperature reached in the TPD experiment), it is likely that carbonate phases formation is avoided. Carbonates are totally released at 900 °C. It is thus reasonable that those revealed by means of DRIFT analysis and observed to decompose in the TPD experiment, are essentially a superficial contamination caused by the interaction with atmospheric carbon dioxide. Consistently, the XRD analyses confirm the absence of carbonate phases. The different XPS composition determined for LSGF Gel and Pec can explain the formation of different types of bulk-like carbonates (i.e. CO_2 coordinated to different cations), characterized by a slightly different desorption/decomposition temperature. At this purpose two points should be considered: first, as already observed, La is present in higher amount in LSGF Pec surface while Sr is more evident in LSGF Gel; second the standard Gibbs free energy of formation for lanthanum carbonate is a lot more favourable than the corresponding value of strontium carbonate (the Gibbs free energy of formation of the other carbonates are even less favourable). Taking also into account the basic character of these elements, it is reasonable to suppose that the main cause for carbonates formation is due to lanthanum and strontium. These results suggest that the contribution at about 715 °C in LSGF Pec can thus be ascribed to carbonated species related to lanthanum, while the broad contribution observed in LSGF Gel to carbonates involving strontium [60].

In order to describe the oxidation state and the sites geometry of the Fe nuclei room temperature (RT) and 11 K Mössbauer measurements are performed on two LSGF samples, the as prepared one and the one reduced with methanol vapors at 200 °C. For sake of brevity only LSGF Pec outcomes are discussed; LSGF

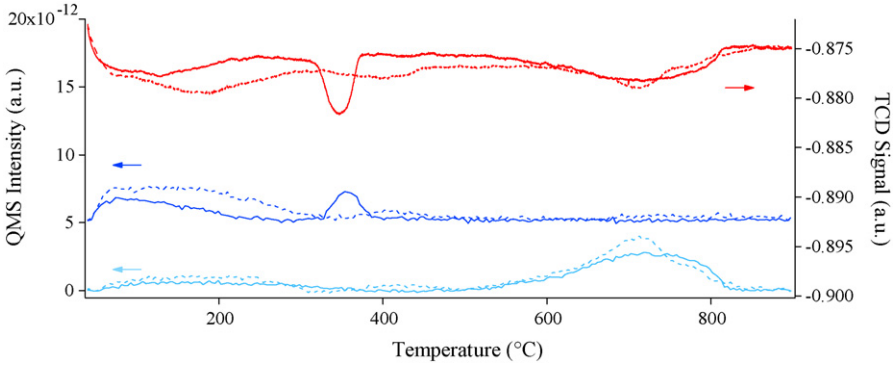

Fig. 4. TPD–QMS outcomes for LSGF Gel (solid line) and LSGF Pec (dashed line). TCD signal (red), H_2O, m/z = 18 (blue), CO_2, m/z = 44 (light blue). The intensities of CO_2 signals are magnified 5 folds. (For interpretation of the references to color in this figure legend, the reader is referred to the web version of the article.)

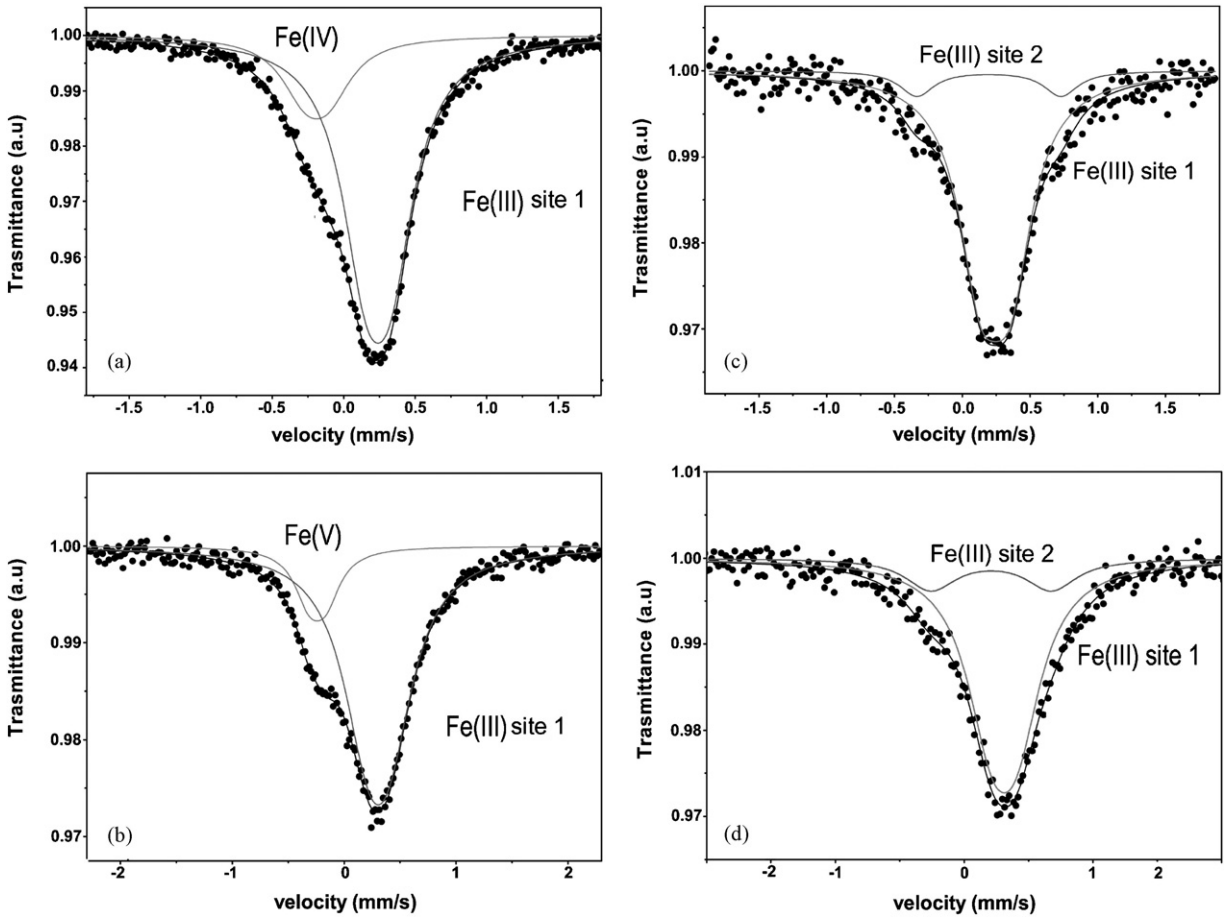

Fig. 5. Mössbauer spectra obtained for LSGF Pec: (a) as prepared RT, (b) as prepared at 11 K; (c) after reduction (with methanol at 200 °C for 1 h) at RT, and (d) at 11 K.

Gel sample gives the same results. The as prepared LSGF Pec gives a single line spectrum centred near zero velocity with a broadening towards negative velocity values, as Fig. 5a shows. The best fitting was achieved by using two components: one due to Fe(III), hereafter site 1, and one due to Fe(IV). Both species occupy high symmetry octahedral sites (Mössbauer parameters are reported in Table 4). The presence of unusual valence states for transition elements is quite common in perovskite-based materials; this was also observed for Fe(IV) in aliovalently doped compounds [64,65]. As known, the substitution of La(III) with Sr(II) creates a deficiency in the positive charges which can be balanced by oxygen vacancies or by increasing the oxidation state of some elements. In this case, it is reasonable to suppose that iron reaches a higher oxidation state (IV), to compensate the excess of negative charges due to Sr(II) in LSGF sample.

The temperature dependence of the Mössbauer parameter is useful to describe more exhaustively the sites occupancy and the oxidation states. 11 K measurement in fact, still show the presence of two distinct sites, two narrow doublets attributed, respectively, to Fe(V) and Fe(III) species (Fig. 5b). The presence of Fe(V) specie is due to the Fe (IV) disproportion according with $2Fe(IV) \rightarrow Fe(III) + Fe(V)$ [64]. In fact, the hyperfine parameters of the ferric site are congruent with those of site 1, with the exception of the relative area that increases as consequence of the Fe(IV) disproportion. The outcomes suggest that Fe(IV) is about 20% of the total iron amount.

The Mössbauer spectrum of the reduced LSGF Pec shows a broad absorption near zero velocity values. The best fitting was achieved by two Fe(III) sites, site 1 and site 2 hereafter, differing each other by the sites symmetry (Fig. 5c). The low temperature measure does not show any significant variations (Fig. 5d). Mössbauer data suggest that the reduction involves only Fe(IV) site which transforms, after the reaction with methanol, into the distorted octahedral site 2. On the other hand the hyperfine parameters of the ferric site in LSGF Pec as prepared are retained (in site 2 of LSGF Pec after reduction). A comparison between the relative area of Fe(IV) and the area of site 2, in the low temperature measure of the reduced sample, confirms the hypothesis. The small variation between the RT and low temperature measure areas is ascribed to the dependence of the resonant fraction, *f*, from the measure temperature.

In order to get more information concerning iron oxidation states in LSGF, the UV–Vis spectra of the as prepared samples were compared with the corresponding ones obtained for a sample reduced by treating with methanol at 200 °C (Fig. 6).[1]

The analysis of the optical spectra of the as prepared and reduced LSGF Pec (Fig. 6) confirms the partial oxidation of Fe(III) to Fe(IV) when Sr(II) replaces La(III) in the LSGF. In the spectrum of the reduced sample, in fact, the optical bands characteristic of Fe(III) ions in octahedral coordination are evident, as expected for the d–d transitions and ligand to metal charge transfer (CT) [66–71]. A different shape characterizes the UV–Vis spectrum of the as prepared

[1] As a consequence of the treatment the sample colour changes from the original dark brown-black to light brown-ochre. Moreover, the reaction seems to be completely reversible. In fact, the reduced sample goes back to the original conditions when exposed to pure oxygen atmosphere at 200 °C for 5 h. The XPS and XRD measurements carried out on the reduced (sample treated with methanol vapours at 200 °C for 1 h) and re-oxidized (treating the reduced sample with pure O_2 at 200 °C for 5 h) LSGF Pec and Gel show no differences with respect to the as prepared samples.

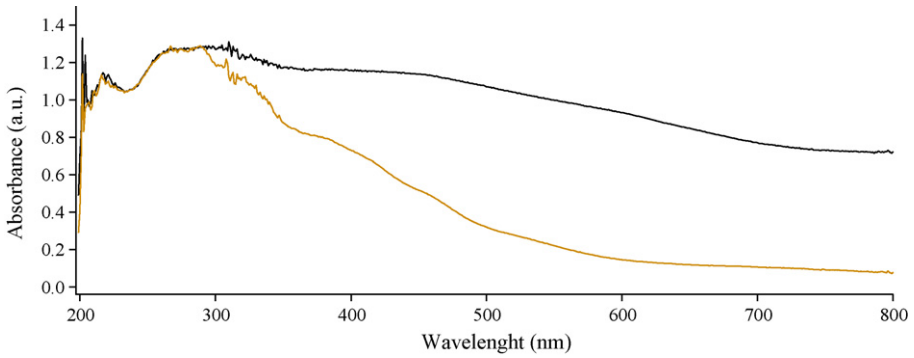

Fig. 6. Diffuse reflectance UV–Vis spectra obtained for LSGF Pec as prepared (black) and after treatment with CH_3OH at 200 °C for 1 h (ochre). (For interpretation of the references to color in this figure legend, the reader is referred to the web version of the article.)

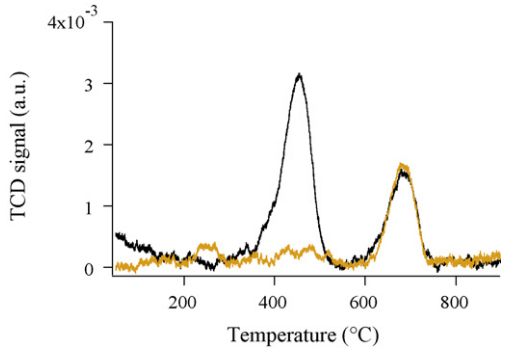

Fig. 7. TPR outcomes obtained for LSGF Gel as prepared (black) and reduced with methanol at 200 °C for 1 h (ochre). (For interpretation of the references to color in this figure legend, the reader is referred to the web version of the article.)

LSGF, which, as above mentioned, contains about 20% of Fe(IV) in addition to Fe(III). The spectra of the as prepared and reduced samples, in fact, are fully superimposable in the region between 200 and 300 nm (where only the absorptions of Fe(III) occur), while they differ at higher wavelength. A great absorption characterizes the spectrum of the as prepared LSGF. When Fe(IV) is present, in fact, because of its great oxidizing power, the ligand to metal charge transfer bands dominate the spectrum obscuring the low intensity d–d adsorptions [72].

Fig. 7 shows the TPR results obtained for LSGF Gel as prepared. The peak at about 450 °C is ascribed to the reduction of Fe(IV) to Fe(III). The theoretical hydrogen consumption (2.00 ml/g at standard temperature and pressure, STP), well agrees with the experimental value (1.95 ml/g STP), confirming the hypothesis. The second peak, at about 670 °C, can be due to a partial reduction of Fe(III) to Fe (II). The TPR analysis was also carried out on a LSGF Gel sample pre-treated with methanol (at 200 °C for 1 h): in this case the peak due to the reduction of Fe(IV) to Fe(III) disappears and only the second peak is still present.

The comparison with literature data suggests that the reduction of Fe(IV) to Fe(III) and Fe(III) to Fe(II) in LSGF occurs at higher temperature than how usually observed. For example, in doped $LaFeO_3$. Fe(IV) is reduced to Fe(III) at temperatures lower than 300 °C, Fe(III) to Fe(II) at about 460 and 570 °C (surface and bulk atoms respectively) and the reduction of Fe(II) to metallic Fe occurs at temperatures above 700 °C [67,73,74].

4.2. Reactivity tests

4.2.1. Methanol and ethanol vapours

The QMS and IR data are reported in Figs. 8 and 9, respectively for methanol and ethanol. The catalysts begin to be active with

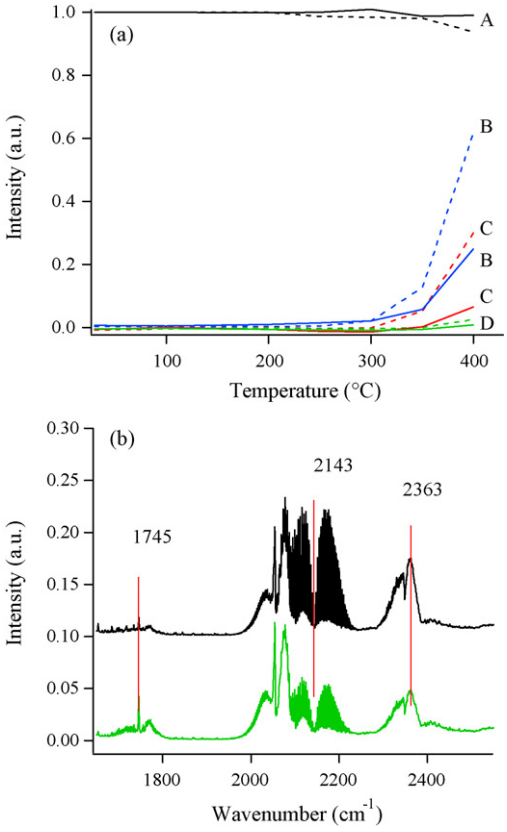

Fig. 8. (a) QMS data obtained for m/z = 29 (methanol black A), m/z = 2 (hydrogen blue B), m/z = 28 (carbon monoxide red C) and m/z = 44 (carbon dioxide green D) at the investigated temperatures in the test with pure methanol vapours. The intensities of m/z = 2, 28 and 44 are magnified 3 folds. Solid lines stand for LSGF Gel, dashed lines for LSGF Pec. All mass data are normalized with respect to methanol intensity. (b) FTIR spectra obtained after exposing LSGF Gel (green) and LSGF Pec (black) to methanol vapours (effluent gas from the reactor) at 400 °C. Region between 1650 and 2550 cm^{-1}. The spectra are y-shifted for a better comprehension. (For interpretation of the references to color in this figure legend, the reader is referred to the web version of the article.)

respect to methanol, at temperature of 300–350 °C, H_2 and CO are the main products at all temperatures and for both the samples. The catalyst activity and the amounts of the observed products increase with increasing temperature and they are higher for the catalyst obtained by means of the Pechini procedure. The observed products suggest that, under the operating conditions, methanol mainly undergoes to decomposition (Eq. (10)) into H_2 and CO.

The activity improves at 400 °C, when an increase of the CO and H_2 amounts is observed. At this temperature, CO_2 and traces

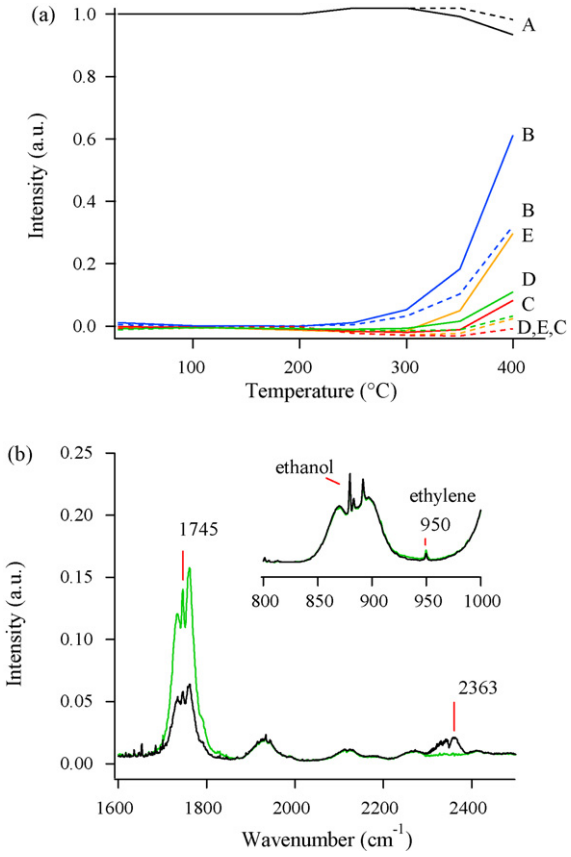

Fig. 9. (a) QMS data for m/z = 31 (ethanol black A), m/z = 29 (acetaldehyde ochre E) m/z = 2 (hydrogen light blue B), m/z = 44 (carbon dioxide green D) and m/z = 28 (carbon monoxide and ethylene red C) obtained at the investigated temperatures, in the test with pure ethanol vapours. The intensities of m/z = 2, 28, 29 and 44 are magnified 3 folds. Solid lines stand for LSGF Gel, dashed lines for LSGF Pec. All mass data are normalized with respect to ethanol intensity. (b) FTIR spectra obtained after exposing LSGF Gel (green) and LSGF Pec (black) to ethanol vapours (effluent gas from the reactor) at 400 °C. Region between 1600 and 2500 cm^{-1}. Insert: region between 800 and 1000 cm^{-1}. (For interpretation of the references to color in this figure legend, the reader is referred to the web version of the article.)

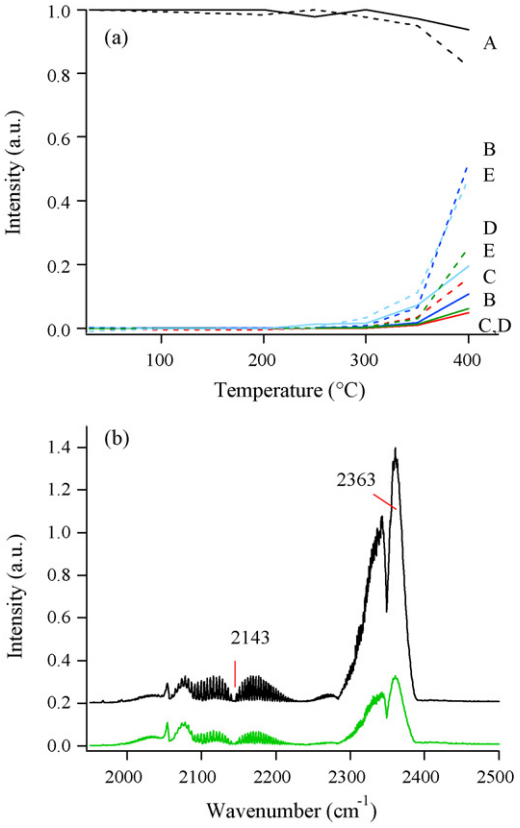

Fig. 10. (a) QMS data obtained for m/z = 29 (methanol black A), m/z = 2 (hydrogen blue B), m/z = 28 (carbon monoxide red C), m/z = 44 (carbon dioxide green D) and m/z = 18 (water light blue E) in oxidizing conditions with methanol at the investigated temperatures. Solid lines stand for LSGF Gel, dashed lines for LSGF Pec. All mass data are normalized with respect to methanol intensity. (b) FTIR spectra obtained after exposing LSGF Gel (green) and LSGF Pec (black) to methanol vapours in oxidizing conditions (effluent gas from the reactor) at 400 °C. Region between 1950 and 2500 cm^{-1}. The spectra are y-shifted for a better comprehension. (For interpretation of the references to color in this figure legend, the reader is referred to the web version of the article.)

of formaldehyde and methyl formate (Fig. 8b, IR peak at about 1745 cm^{-1}) are also detected. The formation of CO_2 and H_2CO can involve the hydroxyl groups, as already observed on several oxides [75–81] or lattice oxygen [82]. The catalyst reduction observed after exposure to methanol at increasing temperatures [65] seems to support this last hypothesis.

Carbon dioxide can also arise from the Boudouard reaction Eq. (25) [83]. Nevertheless, this reaction is favoured at higher temperature and its contribution to the overall CO_2 production can be assumed quite low.

LSGF samples react with ethanol vapours starting from 300 °C. As revealed by QMS data (Fig. 9a) and by IR spectra (Fig. 9b), at this temperature only very small amounts of hydrogen and acetaldehyde (IR signal at 1745 cm^{-1}) are detected. The temperature increment (until 350 and 400 °C) favours the increase of the activity. The observed species are consistent with the dehydrogenation of ethanol Eq. (16).

At 400 °C traces of ethylene are also detected for both compounds; LSGF Pec, furthermore, produces a small amount of CO_2. Literature references suggest that ethylene can be obtained from ethyl alcohol when acidic catalysts are employed Eq. (26); in general, alcohols undergo dehydration to olefins and ethers over acidic catalysts and dehydrogenation to aldehydes or ketones over basic catalysts [84]. In some cases, however, heterogeneous basic catalysts promote alcohols dehydration with mechanisms and a products distribution different from those of acid-catalyzed dehydration. Such behaviour was observed, as an example, over zirconia and rare earth oxides [85]. Sheng et al. [86], nevertheless, indicate that sub-stoichiometric oxides also can promote ethanol dehydration. In this case, however, ethylene (whose presence should be avoided to prevent coke formation Eq. (27)) is observed only when the catalysts interact with the alcohol vapours; moreover, in spite of the different surface composition (as revealed by XPS measurements) the same behaviour is observed for the two samples. These results suggest that the experimental conditions are mainly responsible of the ethylene formation.

Both samples appear scarcely active with respect to methanol and ethanol. Table 5 shows the conversions of the alcohols. The yields for the products cannot be easily calculated because of the multiple reaction pathways (i.e. formation of by-products) [87]. Nevertheless, the obtained H_2/converted methanol ratios (Table 5) suggest a slightly higher hydrogen production for LSGF Gel. The H_2/converted ethanol ratio confirms ethanol dehydrogenation (reaction Eq. (16)) as main reaction for both catalysts.

4.2.2. Methanol and ethanol oxidation

The oxidation tests were performed by feeding the reactor with the alcohol vapours carried by a mixture Ar–O_2 (oxygen to methanol ratio = 1.7; oxygen to ethanol ratio = 3.3). The results obtained for methanol oxidation (Fig. 10) indicate that both samples are not active until 300 °C. From 350 °C on, signals arising from

Table 5
Conversions of fuels and H_2 obtained/alcohol converted molar ratios at 400 °C for LSGF Gel and Pec with respect to the investigated conditions.

Conditions/reactants	Alcohols conversions (%)		H_2 obtained/alcohol converted	
	LSGF Gel	LSGF Pec	LSGF Gel	LSGF Pec
CH_3OH	2	7	1.1	0.8
CH_3CH_2OH	5	2	0.7	0.8
$CH_3OH–O_2$	6	18	0.7	1.1
$CH_3CH_2OH–O_2$	13	14	0.2	0.7
CH_3OH 1 M	23	12	2.8	2.1
CH_3CH_2OH 1 M	28	16	5.4	5.9

H_2, CO, CO_2 and H_2O appear (QMS data, Table 5 and Fig. 10a). Besides QMS, the formation of CO_2 is evident from the IR peak at 2363 cm^{-1}, while CO presence was confirmed by IR band centred at 2143 cm^{-1} (Fig. 10b). All the products increase with temperature rise. Traces of formaldehyde cannot be excluded.

The obtained products and the comparison between the amounts of H_2 and CO, toward H_2O and CO_2, suggest the coexistence of different reaction patterns. Probably, the complete oxidation Eq. (3) competes with the methanol partial oxidation reactions (Eqs. (4) and (5)). It is worth to point out that methanol decomposition Eq. (10) also gives the same products (H_2 and CO). Nevertheless, the quite low values obtained for the conversion of pure methanol vapours (Table 5), and, as a consequence, the small amounts of hydrogen and carbon monoxide obtained from this path, allow thinking that the methanol decomposition does not contribute significantly to the overall amount of CO and H_2.

The conversion data shown in Table 5, indicate that LSGF Pec is more active than LSGF Gel in methanol oxidation. Anyway, the H_2/converted alcohol ratios (Table 5), suggest that LSGF Gel promotes water formation better than LSGF Pec (lower amount of H_2 among products). Carbon-containing intermediates, otherwise, are more easily converted into CO_2 by LSGF Pec (0.5 moles of CO_2 obtained per mole of methanol) than by LSGF Gel (0.3).

Also in ethanol oxidation, in LSGF Gel the formation of wateris more favoured than in LSGF Pec (see H_2/converted ethanol ratios in Table 5). Consistently, the carbon dioxide formation is 0.1 and 0.4 moles per mole of converted ethanol for LSGF Gel and Pec respectively.

This different attitude toward oxidation was confirmed by the results of further investigations: the activity of LSGF Pec with respect to hydrogen oxidation (a mixture H_2/Ar + O_2 was employed) and carbon monoxide oxidation (using a mixture CO + O_2) indicates that the conversion of hydrogen into water is negligible, while CO is oxidized to CO_2 with a conversion of about 15% and almost 100% selectivity to CO_2.

Interesting results were observed carrying out the reactions under different conditions (repeated activity tests). Concerning this, LSGF Pec, as an example, was investigated directly at 400 °C with respect to methanol oxidation. The outcomes appear remarkable: methanol conversion reaches about 82%. Under these conditions, mainly the total oxidation reaction occurs and CO_2 is produced with about 70% yield and only 15% of H_2 is observed. Successively, other five cycles have been repeated and the methanol conversion decreases approaching the values observed in the previous test (18%). Noteworthy, the activity of the catalysts does not significantly decrease with time during the investigation at each temperature. The deactivation observed during the subsequent cycles, can be attributed to the interaction of the reaction products (CO_2) and intermediates (formate) with the catalyst surface. To better investigate this aspect, the worn-out catalysts derived from the reactions carried out at increasing temperatures, were investigated with DRIFT spectroscopy after the reaction with $CH_3OH–O_2$, $CO–O_2$ and $H_2–O_2$ (Fig. 11) in order to understand the contributions to the poisoning coming from the different species. The spectrum

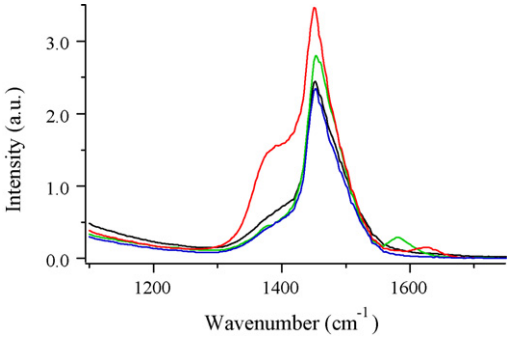

Fig. 11. DRIFT spectra obtained for the worn-out LSGF Pec samples after the catalytic tests with CO + O_2 (red), H_2 + O_2 (blue), CH_3OH + O_2 (green). The spectrum of the as prepared sample is also shown for comparison (black). (For interpretation of the references to color in this figure legend, the reader is referred to the web version of the article.)

obtained after exposure to $H_2–O_2$ shows no significant differences with respect to the un-reacted sample (in agreement with the negligible activity). On the other hand, the sample after exposure to CO + O_2 shows a carbonate groups increment. The peak at about 1625 cm^{-1} is due to moisture. The spectrum of the sample after the test with $CH_3OH–O_2$ exhibits an increase in the signal due to monodentate carbonates whereas a new contribution at about 1580 cm^{-1} can be assigned to adsorbed formate, although a contribution from bidentate carbonate cannot be excluded.

It is reasonable to think that most of the residual carbonates, mainly monodentate carbonate species, derives from the interaction of carbon dioxide with oxygen anions near neighbours of lanthanum or strontium cations. Bulk-like carbonates form with increasing the CO_2 adsorption. Since the amount of adsorbed species appears quite high (with respect to the content of carbon-containing species in the effluent stream from the reactor), and the activity of the samples does not decrease significantly, the reactivity of the perovskite materials is mainly due to the B-site cations, as suggested by many Authors [88,89].

Taking into account, beside the DRIFT data (Fig. 11), the outcomes from the repeated activity tests (at 400 °C) and those obtained at increasing temperature (Fig. 10), it appears that the surface poisoning occurs whenever the reaction is interrupted (stopping the reactants flow, thus interrupting reactants feed). It is thus probable that the high temperature locally reached during the reaction (caused by the exothermic reactions), is enough to cause the desorption of most of carbon dioxide, thus avoiding the surface deactivation (this mechanism loses its efficacy whenever the reaction slows down, and then the temperature drop down).

It is interesting, however, to observe that defective gallia surfaces (for the presence of oxygen vacancies, as an example) obtained by heat treatments in absence of oxygen, show a lower reactivity with respect to methanol [90].

Regarding ethanol oxidation, LSGF samples show no activity until 300 °C: at this temperature small traces of hydrogen and acetaldehyde can be detected. At 400 °C (Fig. 12a and b for QMS

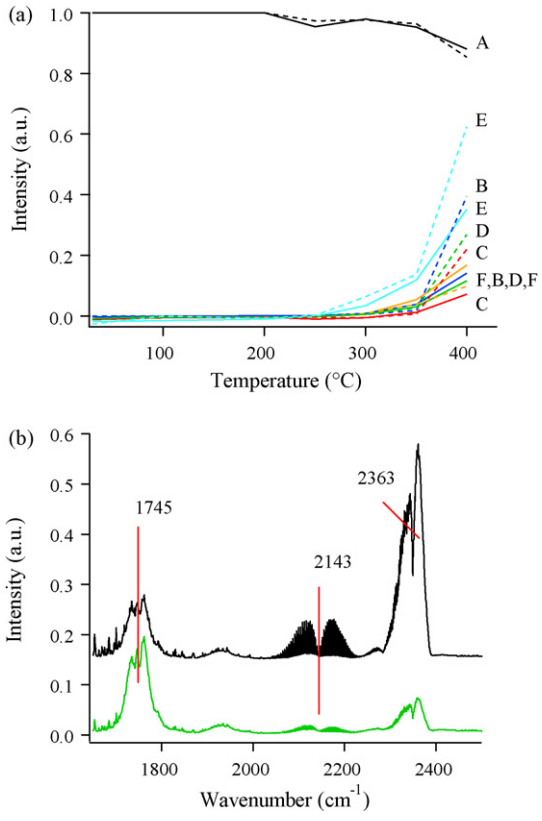

Fig. 12. (a) QMS data obtained for m/z = 31 (ethanol black A), m/z = 29 (acetaldehyde ochre F), m/z = 2 (hydrogen blue B), m/z = 28 (carbon monoxide red C), m/z = 44 (carbon dioxide green D) and m/z = 18 (water light blue E) in oxidizing conditions with ethanol. Solid lines stand for LSGF Gel, dashed lines for LSGF Pec. All mass data are normalized with respect to ethanol intensity. (b) FTIR spectra obtained after exposing LSGF Gel (green) and LSGF Pec (black) to ethanol vapours in oxidizing conditions (effluent gas from the reactor) at 400 °C. Region between 1650 and 2500 cm^{-1}. The spectra are y-shifted for a better comprehension. (For interpretation of the references to color in this figure legend, the reader is referred to the web version of the article.)

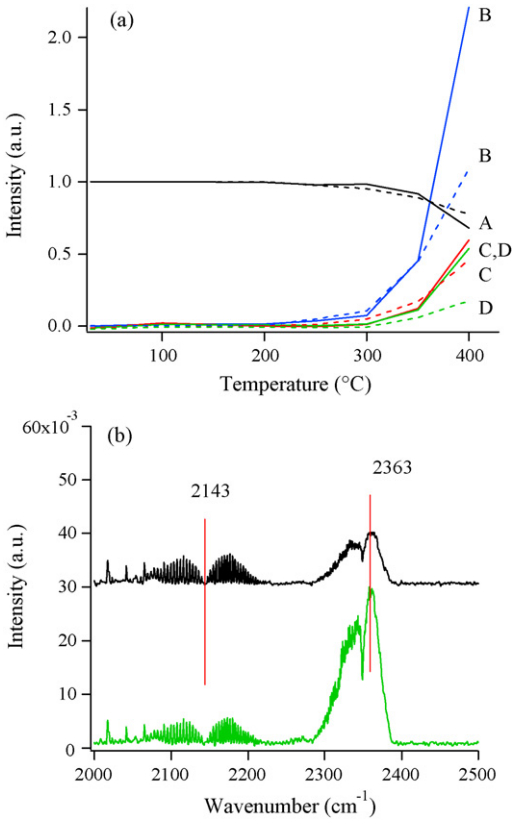

Fig. 13. (a) QMS data obtained for m/z = 29 (methanol black A), m/z = 2 (hydrogen blue B), m/z = 28 (carbon monoxide red C), and m/z = 44 (carbon dioxide green D) in methanol steam reforming tests. Solid lines stand for LSGF Gel, dashed lines for LSGF Pec. All mass data are normalized with respect to methanol intensity. (b) FTIR spectra obtained after exposing LSGF Gel (green) and LSGF Pec (black) to CH_3OH 1M vapours (effluent gas from the reactor) at 400 °C. Region between 2000 and 2500 cm^{-1}. The spectra are y-shifted for a better comprehension. (For interpretation of the references to color in this figure legend, the reader is referred to the web version of the article.)

and IR data respectively) the amounts of these products increase and new QMS and IR signals ascribable to H_2O, CO (IR band centred at 2143 cm^{-1}), and CO_2 (2363 cm^{-1}) appear, suggesting a more relevant contribution from ethanol oxidation.

Quantitative data shown in Table 5 suggest that both LSGF Gel and Pec reach the same performances concerning ethanol conversion. The obtained products, in particular acetaldehyde (Fig. 12b, band at 1745 cm^{-1}) and H_2, agree with ethanol dehydrogenation Eq. (16). Several other products, such as carbon monoxide, carbon dioxide, methane, acetone and ethyl acetate, are observed by different Authors, as a function of the catalyst, when ethanol reacts in the presence of oxygen; these products are consistent with the different reaction path (see Section 1) [2,84,86,91]. Since only H_2, H_2O, CH_3CHO, CO and CO_2 have been observed in the present case, it is probable that only few reaction paths have to be considered beside dehydrogenation Eqs. (6, 7, 9, 11, 18, 21); moreover, the amounts of "C1" species appear quite low, suggesting that the C–C bond break limits the reaction rate.

4.2.3. Methanol and ethanol steam reforming

LSGF Pec and Gel start to convert methyl alcohol from 350 °C under steam reforming conditions. The observed products are mainly H_2, CO and CO_2, which agree with the steam reforming of methanol Eq. (1). Fig. 13a and b shows the obtained QMS and IR results. The presence of carbon monoxide is easily explained assuming the steam reforming reaction as the sum of methanol decomposition Eq. (10) followed by the water gas shift reaction Eq. (11) [83].

LSGF catalysts become active toward ethanol steam reforming since 300 °C, when only weak signals for m/z = 2 (hydrogen), and m/z = 28 (carbon monoxide and ethylene) are detected (Fig. 14a and b for QMS and IR data respectively). The increase of the temperature at 350 and 400 °C emphasizes the activity with a larger production of H_2 and CO_2 (IR band at 2363 cm^{-1}, Fig. 14b). Unlike how observed for LSGF Pec, acetaldehyde also forms during the test with LSGF Gel (IR signals at 2705 and 2731 cm^{-1}, Fig. 14b).

Quantitative values for the conversions of the alcohols at 400 °C are summarized in Table 5. From these data it can be seen that both catalysts appear more active toward the reforming of the fuels compared to the values for pure alcohols and alcohols oxidation. Nevertheless, it should be considered that the feed conditions are different, and lower WHSV are employed in steam reforming tests (Table 1).

The H_2 produced/alcohol converted ratios (Table 5) allow further considerations. In methanol steam reforming, LSGF Gel produces 2.8 moles of H_2 per mole of CH_3OH converted versus 2.1 for LSGF Pec. The values suggest that LSGF Gel works near to the full reforming (3 is the maximum value). On the other hand, in LSGF Pec a different reactivity is observed and it seems to promote methanol decomposition (2 is the value when only CH_3OH decomposition occurs), while the Water Gas Shift Reaction (WGSR, Eq. (11)) appears slow. Nevertheless, especially for LSGF Pec, no cer-

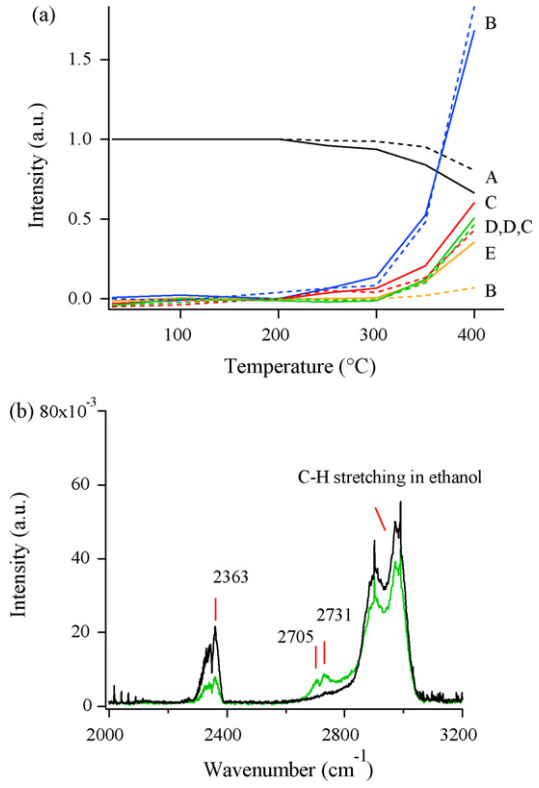

Fig. 14. (a) QMS data obtained for m/z = 31 (ethanol black A), m/z = 29 (acetaldehyde ochre E) m/z = 2 (hydrogen blue B), m/z = 44 (carbon dioxide green D) and m/z = 28 (carbon monoxide and ethylene red C) in ethanol steam reforming tests. Solid lines stand for LSGF Gel, dashed lines for LSGF Pec. All mass data are normalized with respect to ethanol intensity. (b) FTIR spectra obtained after exposing LSGF Gel (green) and LSGF Pec (black) to CH_3CH_2OH 1 M vapours (effluent gas from the reactor) at 400 °C. Region between 2000 and 3200 cm^{-1}. (For interpretation of the references to color in this figure legend, the reader is referred to the web version of the article.)

tain conclusions can be made, since the carbon containing species retained on the catalysts do not allow a stoichiometric calculation.

Concerning ethanol reforming, both catalysts approach to the maximum value for H_2 produced/ethanol converted (i.e. 6). Nevertheless, LSGF Gel gives also a small amount of acetaldehyde and a lower H_2 production is observed.

For both samples a mismatch between the alcohols conversion values and the amount of carbon containing species is observed (only about 0.1 moles of CO and CO_2 are obtained per mole of converted alcohol). Consistently, a quite large amount of carbonate species is retained on the catalysts surface.

To verify the poisoning effect on the activity of the catalysts, LSGF Pec was investigated directly at 400 °C in repeated reaction cycles. During the first cycle, methanol conversion reaches 17%, such as in the second one. In the third cycle it decreases to 16% and to 15% in the fourth.

Table 6 resumes the methanol conversions and the amounts of hydrogen, carbon monoxide and carbon dioxide obtained per mole of converted methanol. From Table 6, it can be seen that the amounts of CO and CO_2 produced (and released) per mole of converted methanol become lower from cycle 1 to 4, while the amount of H_2 remains essentially the same. This suggests that the mechanism of the reaction is not modified by the activity decrease, but it indicates that more carbon-containing species are retained on the catalyst.

The mismatch between the methanol conversion observed in the test carried out at increasing temperatures from RT to 400 °C, 12%, and the value obtained in the first cycle (17%) allows to state that also in this case the catalyst performance is affected by the tests at increasing temperature. At this purpose the possibility to create defective sites has to be considered as well as the poisoning effect of the unreleased species (mainly carbonates) adsorbed on the surface active sites (at this purpose the steric hindrance of adsorbed species, such as CO_2 as example, has also to be considered).

The mechanisms proposed for alcohols reactions over metal oxides or mixed metal oxides differ as a function of the catalysts. Accordingly to literature, the first step of alcohol decomposition, oxidation and/or steam reforming on metal oxides is the interaction with the surface; this interaction can be molecular or dissociative, depending on the alcohol acidity and on the acidic/basic character of the oxide. The following steps take into account the subsequent dehydrogenation of methoxy groups and the formation of intermediate species such as formaldehyde, methyl formate or dioxomethylene. Finally, the decomposition or oxidation products are desorbed from the surface. The small amounts of monodentate (~1640 cm^{-1}) and bidentate formate (~1585 cm^{-1}) [92] observed (by means of DRIFT spectroscopy) on the catalysts (at RT and 100 °C) after methanol chemisorption, confirm this mechanism. Consistently, chemisorption of ethyl alcohol shows traces of acetate species at about 1541 cm^{-1} at 100 °C [93].

The next step after alcohol interaction is the methyl (or methylene) hydrogen abstraction; this is considered the Rate Determining Step (RDS) in alcohol reactions [85]. As suggested by literature this step can be favoured by the presence of metallic clusters or basic active sites (coordinatively unsaturated oxygen anions, hydroxyl groups) [85,94–98]. In the present case the existence of metallic clusters is unlike, being not in agreement with the preparation procedure or with the XPS results. The rather low reactivity of the samples with respect to the pure alcohols suggests a scarcely relevant presence of free and accessible acidic and basic sites. Further work is in progress to test the influence of the dopants on the acidic and basic sites amount and distribution [99]. Some basic sites could form as a consequence of the water and/or carbon dioxide desorption: TPD results indicate that molecularly adsorbed water desorbs at rather low temperature, whereas tightly bonded water only desorbs at higher temperature (350–400 °C) and 600–800 °C are necessary for carbon dioxide desorption.

Another point to be considered is that the catalyst reactivity increases when oxygen is added; at this purpose it is interesting to observe the reaction mechanism proposed by Tatibouët [100] for methanol oxidation. Taking into consideration the behaviour of several oxides, Tatibouët suggested that the presence of oxygen can help the methyl hydrogen abstraction. In general, several mechanisms are proposed for oxygen activated methanol oxidation [92,94,96,101,102] usually (as revealed by TPD investigation) two different kind of oxygen species are suggested in perovskites: the first one, indicated as α-oxygen, is considered to desorb from the surface of the solid at rather low temperature (<500 °C); the second one, β-oxygen, is supposed to originate from the bulk of the solid (as O^{2-}) and desorbs at high temperature (600–900 °C) with the simultaneous reduction of cations. Two different reaction mechanisms have thus been proposed for perovskites oxidation reactions involving these oxygen species [103,104]: for low-temperature reactions (such as CO oxidation) a suprafacial mechanism with the participation of surface oxygen is suggested, whereas for high temperature reactions an intrafacial mechanism involving lattice oxygen is preferred.

In the present case, the desorption of these species was not observed either in the as prepared sample or in the sample treated in oxygen at 900 °C for 2 h. It is thus probable that oxygen reactivity follows a different mechanism. In general the amount of reversibly

Table 6
Conversions of CH_3OH and amounts of H_2, CO and CO_2 obtained per mole of converted alcohol at 400 °C for LSGF Pec in the cycles of steam reforming.

Conditions	Alcohols conversions (%)	H_2 obtained/CH_3OH converted	CO obtained/CH_3OH converted	CO_2 obtained/CH_3OH converted
400 °C cycle 1	17	2.0	0.4	0.3
400 °C cycle 2	17	2.0	0.4	0.2
400 °C cycle 3	16	2.0	0.3	0.2
400 °C cycle 4	15	1.9	0.2	0.1

adsorbed oxygen in perovskites represents a very small fraction of the total adsorption [105]. It is likely that oxygen adsorption can induce the formation of new basic sites capable of favouring methyl hydrogen abstraction. A similar effect can be ascribed to water whenever present in the reaction mixture. An interesting mechanisms, different with the local surface chemical environment, was observed by Branda et al. [90] in Gallium containing oxides. The (1 0 0) Ga_2O_3 surface without oxygen vacancies, as an example, was observed to be very reactive producing oxidative decomposition of the methanol molecules while non-dissociative adsorption was revealed on the gallia surface with oxygen vacancies. In the present case, the investigate samples show a surface composition which differs with the preparation procedure; consistently, oxygen vacancies and defects may play a different role in determining the activated methyl hydrogen abstraction. The effect of water molecules has also to be considered. Frank et al. [94] suggested, by means of kinetic studies, the intervention of hydroxyl groups originated by water molecules in the conversion of formaldehyde to formic acid. In general the mechanism of the oxidation and steam reforming of alcohols is not completely clear. At least two mechanisms have been hypothesized: one is a redox process involving the interaction of adsorbed intermediates (CO, formaldehyde) with the oxide surface to form carbon dioxide whereas the surface oxygen vacancies are saturated by oxygen of water [97,106–109]. Another mechanism suggests the formation of formates as a consequence of the interaction between carbon monoxide formed on the surface with the hydroxyl groups distributed on the surface [75–81].

It is worth to underline, however, that, in the present case, both samples appear pale yellow (indicating the reduction of iron from Fe(IV) to Fe(III)) after the steam reforming tests, while they preserve the dark-brown colour after the tests in oxidizing conditions. This feature suggests a significant intervention of bulk oxygen at least in the steam reforming reactions; oxygen from water is never included as lattice oxygen (to replace the oxygen lost during the oxidation of the reactants). In the tests carried out under oxidizing conditions, O_2 as reactant can be adsorbed and directly employed at the surface for the oxidation of the fuels, or diffuse into the structure thus replacing the oxygen anions.

Interesting differences can be observed as a function of the preparation procedure; in particular the experimental results suggest that the sample prepared by Gel method is more active in dehydrogenation reaction, as confirmed by the greater amount of aldehyde (see, as example the reactions with ethanol, Fig. 9b, 12b and 14b). In the sample prepared by Pechini method, oxidation seems favoured (as demonstrated by the higher intensity of the CO_2 IR signals). This different behaviour could be related to the different composition of the surfaces: the Pec sample surfaces, in fact, is richer in iron and poorer in gallium, as confirmed by XPS; the higher oxidative capability can thus be related to the presence of iron. The active role played by iron in the ethanol steam reforming reaction was already observed, as an example, by de la Penã et al. on iron and cobalt containing oxides [110]. The Gel sample, in contrast, is richer in Ga; its behaviour is consistent with literature data suggesting the formation of strong hydrogen sorption sites in gallium containing hybrid catalysts [111]. Sites active toward hydrogen adsorption could be helpful in removing the methyl hydrogen thus helping the RDS. This behaviour is particularly evident in the steam reforming of ethanol. Preliminary investigations concerning the influence of Sr and Fe doping on the reactivity of lanthanum gallate with respect to alcohols suggest a relevant complexity in co-doped perovskites: the reactivity of the double-doped material cannot be explained only taking into consideration the effect produced by the single addition of Sr or Fe [99].

5. Conclusions

A strontium- and iron-doped lanthanum gallate ($La_{0.8}Sr_{0.2}Ga_{0.8}Fe_{0.2}O_3$—LSGF) was prepared by Pechini process (LSGF Pec) and polyacrylamide gel method (LSGF Gel). The samples were characterized by different techniques (XRD, XPS, DRIFT, TPD, TPR, BET, UV-Vis and MS) and the reactivity toward methanol and ethanol was tested (in a U-shaped reactor, investigating the reaction products by means of QMS and IR) under several conditions in order to understand the effect of the synthetic route.

XRD results indicate a higher crystallographic purity for LSGF Pec. On the other hand, LSGF Gel is characterized by a higher specific surface area. XPS outcomes show the typical spectra expected for elements in perovskite structure. It can be observed that strontium tends to be surface segregated (particularly in LSGF Gel), while gallium diffuses into the bulk (particularly in LSGF Pec) and iron is surface segregated in LSGF Pec. DRIFT analyses suggest a slight contamination due to carbonate species; hydroxyl groups and adsorbed water are also present. These species can be removed by thermal treatment until 900 °C (adsorption is reversible). Mössbauer spectroscopy and TPR results are consistent with the presence of a small amount of iron as Fe(IV). Fe(IV) can be reduced to Fe(III) with H_2 5% in Ar (at 450 °C) or with CH_3OH (at 200 °C).

Catalytic tests performed with methanol indicate that the alcohol undergoes decomposition into H_2 and CO, but small amounts of CO_2 are also detected. Ethanol is mainly dehydrogenated to acetaldehyde. The tests carried out in oxidizing conditions reveal the oxidation of the fuels (production of H_2O and CO_2); nevertheless, partial oxidation products such as H_2 and CO are observed. In ethanol oxidation, furthermore, acetaldehyde is an important product. Methanol and ethanol are reformed under steam reforming conditions, producing H_2, CO and CO_2. Moreover, acetaldehyde is still present as a reaction product, thus indicating that the break of C–C bond can be a difficult step. LSGF Gel and LSGF Pec undergo poisoning by carbonate species in the reaction conditions, lowering the conversions of the fuels.

The obtained results suggest that the two employed synthetic procedures give quite similar compounds. Nevertheless, the catalytic tests outcomes point out that the slight differences observed in the characterization allow obtaining different results with respect to the type and relative amounts of the observed reaction products. This feature can be mainly related to the different properties of the sample surfaces.

Acknowledgments

The authors gratefully acknowledge Professor E. Tondello for his helpful discussions. This work was supported by the following research programs: "Ossidi nanostrutturati per applicazioni come elettrodi in dispositivi per l'energetica", Università degli Studi di Padova, and "Promo: Nanostrutture organiche, organometalliche, polimeriche ed ibride: ingegnerizzazione supramolecolare delle proprietà fotoniche e dispositivistica innovativa per optoelettronica", Consorzio Interuniveritario Nazionale per la Scienza e la Tecnologia dei Materiali, INSTM. The authors are also grateful to Dr Pierdomenico Biasi and Dr Nicola Gemo for the thermodynamic calculations.

References

[1] D.R. Palo, R.A. Dagle, J.D. Holladay, Chem. Rev. 107 (2007) 3992.
[2] A. Haryanto, S. Fernando, N. Murali, S. Adhikari, Energ Fuels 19 (2005) 2098.
[3] M. Ni, D.Y.C. Leung, M.K.H. Leung, Int. J. Hydrogen Energy 32 (2007) 3238.
[4] J. Llorca, P. Ramírez de la Piscina, J. Sales, N. Homs, Chem. Commun. 7 (2001) 641.
[5] L.G. Tejuca, J.L.G. Fierro, J.M.D. Tascon, Adv. Catal. 36 (1989) 237.
[6] T. Valdes-Solis, G. Marban, A.B. Fuertes, Catal. Today 116 (2006) 354.
[7] W. Wang, H. Zang, G. Lin, Z. Xiong, Appl. Catal. B 24 (2000) 219.
[8] S. Douvatzides, P. Tsiakaras, Solid State Ionics 136–137 (2000) 849.
[9] S.M. Haile, Acta Mater. 51 (2003) 5981.
[10] K. Yamiaji, T. Horita, M. Ishikawa, N. Sakai, H. Yokokawa, Solid State Ionics 108 (1998) 415.
[11] K. Huang, J.B. Goodenough, J. Alloys Compd. 303 (2000) 454.
[12] G.C. Kostogludis, C. Fitkos, A. Ahmad-Khanlou, A. Naoumidis, D. Stover, Solid State Ionics 134 (2000) 127.
[13] X. Zhang, S. Ohara, H. Okawa, R. Maric, T. Fukui, Solid State Ionics 139 (2001) 145.
[14] T. Ishihara, T. Yamada, H. Arikawa, H. Nischiguchi, Y. Takita, Solid State Ionics 135 (2000) 631.
[15] T. Ishihara, Y. Tsuruta, T. Tokada, H. Nishiguchi, Y. Takita, Solid State Ionics 152–153 (2002) 709.
[16] A. Sin, P. Oldier, Adv. Mater. 12 (2000) 649.
[17] L. Malavasi, M.C. Mozzati, S. Polizzi, C.B. Azzoni, G. Flor, Chem. Mater. 15 (2003) 5036.
[18] A. Douy, Int. J. Inorg. Mater. 3 (2001) 699.
[19] K. Huang, J.B. Goodenough, J. Solid State Chem. 136 (1998) 274.
[20] W. Jin, S. Li, P. Huang, N. Xu, J. Shi, J. Membr. Sci. 170 (2000) 9.
[21] A.C. Tas, P.J. Majewski, F. Aldinger, J. Am. Ceram. Soc. 83 (2000) 2954.
[22] M.P. Pechini, US Patent 3 330 697 (1967).
[23] D.A. Shirley, Phys. Rev. B 5 (1972) 4709.
[24] J.F. Moulder, W.F. Stickle, P.E. Sobol, K.D. Bomben, in: J. Chastain (Ed.), Handbook of X-ray Photoelectron Spectroscopy, Physical Electronics, Eden Prairie, MN, 1992.
[25] http://www.ing.unitn.it/~luttero/maud/.
[26] P. Kubelka, F.Z. Munk, Tech. Phys. 12 (1931) 593.
[27] G. Kortum, Reflectance Spectroscopy, Springer, NY, 1969.
[28] Y. Tsuruta, T. Todaka, H. Nisiguchi, T. Ishihara, Y. Takita, J. Electrochem. Soc. 4 (2001) E13.
[29] J. Yuenyongchaiwat, S. Tantayanon, J. Lou, Y.H. Ma, J. Mater. Sci. 39 (2004) 7067.
[30] I.A. Leonidov, V.L. Kozhevnikov, E.B. Mitberg, M.V. Patrakeev, V.V. Kharton, F.M.B. Marques, J. Mater. Chem. 11 (2001) 1201.
[31] V.V. Kharton, A.L. Shaulo, A.P. Viskup, M. Avdeev, A.I. Kurbakov, E.N. Naumovich, F.M.B. Marques, Solid State Ionics 150 (2002) 229.
[32] R. Polini, A. Falsetti, E. Traversa, O. Schaf, P. Knauth, J. Eur. Ceram. Soc. 27 (2007) 4291.
[33] A. Galenda, M.M. Natile, V. Krishnan, H. Bertagnolli, A. Glisenti, Chem. Mater. 19 (2007) 2796.
[34] S.N. Shkerin, M.V. Kuznetsov, N.A. Kalashnikova, Russ. J. Electrochem. 39 (2003) 591.
[35] Y. Zhu, R. Tan, T. Yi, S. Gao, C. Yan, L. Cao, J. Alloys Compd. 311 (2000) 16.
[36] A.E. Bocquet, P. Chalker, J.F. Dobson, P.C. Healy, S. Myhra, J.G. Thompson, Physica C 160 (1989) 252.
[37] T. Saitoh, T. Mizokawa, A.E. Bocquet, H. Namatame, A. Fujimori, T. Takeda, M. Takano, Surf. Sci. Spectra 6 (1999) 294.
[38] http://srdata.nist.gov.
[39] Unpublished data—Measures carried out on $SrCO_3$ powder (Aldrich 99.9+%).
[40] A. Galenda, M.M. Natile, A. Glisenti, Surf. Sci. Spectra 13 (2006) 31.
[41] V. Kozhukharov, M. Machkova, P. Ivanov, H.J.M. Bouwmeester, R. van Doorn, J. Mater. Sci. Lett. 15 (1996) 1727.
[42] M. Couzi, P.V. Huong, Ann. Chim. 9 (1974) 19.
[43] J.V. Evans, T.L. Whateley, Trans. Faraday Soc. 63 (1967) 2769.
[44] B. Bachiller-Baeza, I. Rodriguez-Ramos, A. Guerrero-Ruiz, Langmuir 14 (1998) 3556.
[45] R. Philipp, K. Fujimoto, J. Phys. Chem. 96 (1992) 9035.
[46] Q. Sun, C.W. Liu, W. Pan, Q.M. Zhu, J.F. Deng, Appl. Catal. A 171 (1998) 301.
[47] K. Pokrovski, J.K. Taek, A.T. Bell, Langmuir 17 (2001) 4297.
[48] F.C. Meunier, D. Tibiletti, A. Goguet, D. Reid, R. Burch, Appl. Catal. A 289 (2005) 104.
[49] M. Daturi, C. Binet, J.C. Lavalley, G. Blanchard, Surf. Interface Anal. 30 (2000) 273.
[50] S.E. Collins, M.A. Baltanas, A.L. Bonivardi, J. Phys. Chem. B 110 (2006) 5498.
[51] V. Bolis, G. Magnacca, G. Cerrato, C. Morterra, Thermochim. Acta 379 (2001) 147.
[52] O.V. Manoilova, S.G. Podkolzin, B. Tope, J. Lercher, E.E. Stangland, J.M. Goupil, B.M. Weckhuysen, J. Phys. Chem. B 108 (2004) 15770.
[53] A.W.A.M. van der Heijden, V. Belliere, L.E. Alonso, M. Daturi, O.V. Manoilova, B.M. Weckhuysen, J. Phys. Chem. B 109 (2005) 23993.
[54] J.C. Lavalley, Catal. Today 27 (1996) 377.
[55] A.A. Tsyganenko, V.N. Filimonov, J. Mol. Struct. 19 (1973) 579.
[56] M.A. Henderson, Surf. Sci. Rep. 46 (2002) 1.
[57] P.A. Thiel, T.E. Madey, Surf. Sci. Rep. 7 (1987) 211.
[58] S.E. Collins, M.A. Baltanas, A.L. Bonivardi, Langmuir 21 (2005) 962.
[59] B. Klingenberg, M.A. Vannice, Chem. Mater. 8 (1996) 2755.
[60] S. Bernal, F.J. Botana, R. Garcia, J.M. Rodriguez-Izquierdo, Thermochim. Acta 66 (1983) 139.
[61] L.G. Tejuca, A.T. Bell, J.L.G. Fierro, M.D. Tascon, J. Chem. Soc. Faraday Trans. 1 83 (1987) 3149.
[62] L.G. Tejuca, A.T. Bell, J.L.G. Fierro, M.A. Pena, Appl. Surf. Sci. (1988) 301.
[63] V. Cortes Corberan, L.G. Tejuca, A.T. Bell, J. Mater. Sci. 24 (1989) 4437.
[64] T. Pedersen, S. Saadi, K.H. Nielsen, S. Mørup, K. Kammer, Solid State Ionics 176 (2005) 1555.
[65] U. Russo, G.J. Long, in: G.J. Long, F. Grandjean (Eds.), Mössbauer Spectroscopy Studies Of The High Oxidation State Of Iron in Mössbauer Spectroscopy Applied To Inorganic Chemistry, vol. 3, Plenum Press, NY, 1989.
[66] P. Porta, S. Cimino, S. De Rossi, M. Faticanti, G. Minelli, I. Pettiti, Mater. Chem. Phys. 71 (2001) 165.
[67] P. Ciambelli, S. Cimino, L. Lisi, M. Faticanti, G. Minelli, I. Pettiti, P. Porta, Appl. Catal. B 33 (2001) 193.
[68] P. Ciambelli, S. Cimino, G. La sorella, L. Lisi, S. De Rossi, M. Faticanti, G. Minelli, P. Porta, Appl. Catal. B 37 (2002) 231.
[69] L. Capek, V. Kreibich, J. Dedecek, T. Grygar, B. Wichterlova, Z. Sobalik, J.A. Martens, R. Brosius, V. Tokarova, Micropor. Mesopor. Mater. 80 (2005) 279.
[70] J. Perez-Ramirez, M.S. Kumar, A. Bruckner, J. Mater. Chem. 223 (2004) 13.
[71] A. Jitianu, M. Crisan, A. Meghea, I. Rau, M. Zaharescu, J. Mater. Chem. 12 (2002) 1401.
[72] A.B.P. Lever, Inorganic Electronic Spectroscopy, second ed., Elsevier, 1984.
[73] R. Zhang, H. Alamdari, S. Kaliaguine, J. Catal. 242 (2006) 241.
[74] B.P. Barbero, J. Andrade Gamboa, L.E. Cadùs, App. Catal. B 65 (2006) 21.
[75] T. Shido, Y. Iwasawa, J. Catal. 141 (1993) 71.
[76] T. Shido, Y. Iwasawa, J. Catal. 136 (1992) 493.
[77] T. Shido, Y. Iwasawa, J. Catal. 129 (1991) 343.
[78] T. Shido, K. Asakura, Y. Iwasawa, J. Catal. 122 (1990) 55.
[79] J. Lavalley, Catal. Today 27 (1996) 377.
[80] G. Jacobs, P.M. Patterson, L. Williams, D. Sparks, B.H. Davis, Catal. Lett. 96 (2004) 97.
[81] M.M. Natile, A. Glisenti, Chem. Mater. 17 (2005) 3403.
[82] H.H. Kung, Transition Metal Oxides: Surface Chemistry and Catalysis, Elsevier, 1989.
[83] N. Laosiripojana, S. Assabumrungrat, Chem. Eng. Sci. 61 (2006) 2540.
[84] R.W. McCabe, P.J. Mitchell, Ind. Eng. Chem. Prod. Res. Dev. 23 (1984) 196.
[85] H. Hattori, Chem. Rev. 95 (1995) 537.
[86] P.Y. Sheng, G.A. Bowmaker, H. Idriss, Appl. Catal. A 261 (2004) 171.
[87] This can affects the values of the obtained yields and help to justify the mismatches between the conversions and the obtained yields.
[88] D. Ferri, L. Forni, Appl. Catal. B 16 (1998) 119.
[89] S. Royer, D. Duprez, S. Kaliaguine, J. Catal. 234 (2005) 364.
[90] M.M. Branda, S.E. Collins, N.J. Castellani, M.A. Baltanás, A.L. Bonivardi, J. Phys. Chem. B 110 (2006) 11847.
[91] S.M. de Lima, I.O. da Cruz, G. Jacobs, B.H. Davis, L.V. Mattos, F.B. Noronha, J. Catal. 257 (2008) 356.
[92] S.E. Collins, M.A. Baltanas, A.L. Bonivardi, Appl. Catal. A 295 (2005) 126.
[93] J. Rasko, J. Kis, Appl. Catal. A 287 (2005) 252.
[94] B. Frank, F.C. Jentoft, H. Soerijanto, J. Krohnert, R. Schlogl, R. Schomacker, J. Catal. 246 (2007) 177.
[95] S.T. Yong, K. Hidajat, S. Kawi, Catal. Today 131 (2008) 188.
[96] B. Lavasseur, S. Kaliaguine, Appl. Catal. A 343 (2008) 29.
[97] P.O. Graf, D.J.M. de Vlieger, B.L. Mojet, L. Lefferts, J. Catal. 262 (2009) 181.
[98] J. Greeley, M. Mavrikakis, J. Catal. 208 (2002) 291.
[99] Ongoing measurements on $La_{(1-x)}Sr_xGa_{(1-x)}Fe_xO_3$.
[100] J.M. Tatibouët, Appl. Catal. A 148 (1997) 213.
[101] M.M. Branda, G.R. Garda, H.A. Rodriguez, N.J. Castellani, Appl. Surf. Sci. 254 (2007) 120.
[102] G. Busca, A.S. Elmi, P. Forzatti, J. Phys. Chem. 91 (1987) 5263.
[103] S. Royer, F. Bérubé, S. Kaliaguine, Appl. Catal. A 282 (2005) 273.
[104] L. Lisi, G. Bagnasco, P. Ciambelli, S. De Rossi, P. Porta, G. Russo, M. Turco, J. Solid State Chem. 146 (1999) 176.

[105] M.A. Peña, J.L.G. Fierro, Chem. Rev. 101 (2001) 1981.
[106] T. Bunleisin, R. Gorte, G. Graham, Appl. Catal. B 15 (1998) 107.
[107] S. Hilaire, X. Wang, T. Luo, R.J. Gorte, J. Wagner, Appl. Catal. A 215 (2001) 271.
[108] Y. Li, Q. Fu, M. Flytzani-Stephanopoulos, Appl. Catal. B 27 (2000) 179.
[109] S.E. Collins, L.E. Briand, L.A. Gambaro, M.A. Baltanás, A.L. Bonivardi, J. Phys. Chem. C 112 (2008) 14988.
[110] V.A. de la Penã, R.N. O'Shea, P.R. de la Piscina, N. Homs, Int. J. Hydrogen Energy 33 (2008) 3601.
[111] R. Carli, R. Le van Mao, C.L. Bianchi, V. Ragaini, Catal. Lett. 21 (1993) 265.